AD-A112 415 YALE UNIV NEW HAVEN CONN F/G 20/5
TUNABLE WAVELENGTH SOLID-STATE LASERS AND TURBULENT JET DIAGNOS--ETC(U)
SEP 81 R K CHANG AFOSR-77-3433
UNCLASSIFIED AFOSR-TR-82-0135 NL

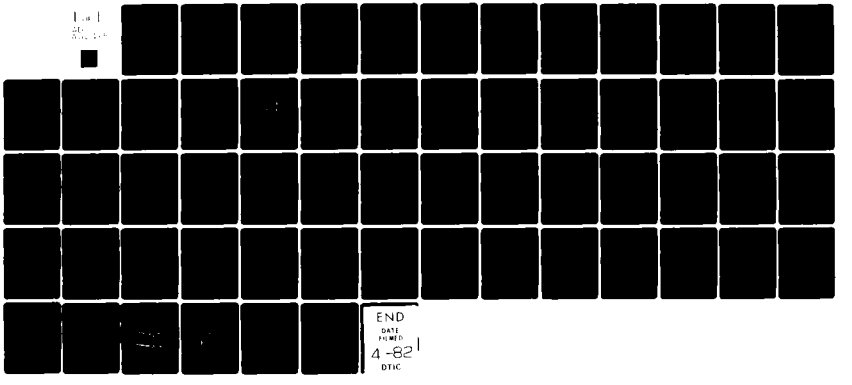

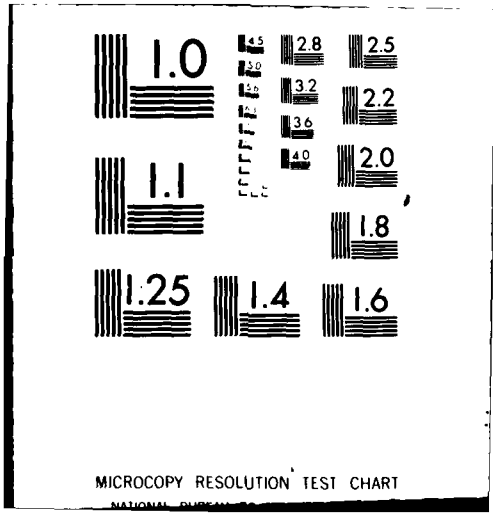
1.0
1.1
1.25
1.4
1.6
1.8
2.0
2.2
2.5
2.8
3.2
3.6
4.0
4.5
5.0
MICROCOPY RESOLUTION TEST CHART

Final Report

to the

Air Force Office of Scientific Research

TUNABLE WAVELENGTH SOLID-STATE LASERS AND TURBULENT JET DIAGNOSTICS BY RAYLEIGH AND FLUORESCENCE SCATTERING

AFOSR [redacted] 77-3433

September 1, 1977 - September 30, 1981

Richard K. Chang, Principal Investigator

Yale University
Applied Physics
New Haven, Connecticut 06520

UNCLASSIFIED

SECURITY CLASSIFICATION OF THIS PAGE (When Data Entered)

REPORT DOCUMENTATION PAGE		READ INSTRUCTIONS BEFORE COMPLETING FORM
1. REPORT NUMBER AFOSR-TR- 82 -0135	2. GOVT ACCESSION NO. AD-A112	3. RECIPIENT'S CATALOG NUMBER 415
4. TITLE (and Subtitle) TUNABLE WAVELENGTH SOLID-STATE LASERS AND TURBULENT JET DIAGNOSTICS BY RAYLEIGH AND FLUORESCENCE SCATTERING		5. TYPE OF REPORT & PERIOD COVERED Final 9/1/77 - 9/30/81
		6. PERFORMING ORG. REPORT NUMBER
7. AUTHOR(s) Richard K. Chang		8. CONTRACT OR GRANT NUMBER(s) AFOSR — 77-3433
9. PERFORMING ORGANIZATION NAME AND ADDRESS Yale University Applied Physics P.O. Box 2157, Yale Station New Haven, CT 06520		10. PROGRAM ELEMENT, PROJECT, TASK AREA & WORK UNIT NUMBERS 61102F (Program Element) 2301/A3
11. CONTROLLING OFFICE NAME AND ADDRESS AFOSR/NP Bolling AFB, Bldg. #410 Wash DC 20332		Sept 1981
		13. NUMBER OF PAGES 56
14. MONITORING AGENCY NAME & ADDRESS(if different from Controlling Office)		15. SECURITY CLASS. (of this report) Unclassified
		15a. DECLASSIFICATION/DOWNGRADING SCHEDULE

16. DISTRIBUTION STATEMENT (of this Report)

Approved for public release; distribution unlimited.

17. DISTRIBUTION STATEMENT (of the abstract entered in Block 20, if different from Report)

18. SUPPLEMENTARY NOTES

19. KEY WORDS (Continue on reverse side if necessary and identify by block number)

Solid-state lasers	Turbulent structures
Tunable lasers	Axisymmetric jets
Excited-state absorption	Rayleigh scattering
Crystal growth	Fluorescence scattering

20. ABSTRACT (Continue on reverse side if necessary and identify by block number)

Broadly tunable solid-state lasers in the blue-green appeared to be feasible for Eu^{2+} and Ce^{3+} ions doped in several host crystals. While the optical absorption and fluorescence were encouraging, our results on excited-state absorption indicated that laser action from many of the crystals considered by our group and other laboratories is not possible. Based on our (Cont'd)

DD FORM 1 JAN 73 1473 EDITION OF 1 NOV 65 IS OBSOLETE

UNCLASSIFIED

SECURITY CLASSIFICATION OF THIS PAGE (When Data Entered)

20. (Cont'd)

results, a general guideline can be established for screening the existence of excited-state absorption from known linear absorption and fluorescence spectra, thereby alleviating the need to perform excited-state absorption experiments for each crystal.

$Ce^{(3+)}$ ions doped in A_2BYF_6 (A = Cs or Rb and B = Na or K) crystals possess low excited-state absorption, broad fluorescence bands in the blue-green, and pump bands easily accessible with N_2 or XeCl lasers. Purification and growth procedures for synthesizing single crystals of Cs_2KYF_6 and Kb_2KYF_6 doped with 0.01% $Ce^{(3+)}$ ions are presented.

Preliminary results on instantaneous two-dimensional concentration mapping of the large-scale coherent turbulent structures from an axisymmetric jet are reviewed. The Rayleigh scattering from the nozzle gas itself and the fluorescence scattering from I_2 molecules seeded in the nozzle gas appear to be viable new optical techniques for turbulence diagnostic studies.

Table of Contents

Abstract

Broadly tunable solid-state lasers in the blue-green appeared to be feasible for Eu^{2+} and Ce^{3+} ions doped in several host crystals. While the optical absorption and fluorescence were encouraging, our results on excited-state absorption indicated that laser action from many of the crystals considered by our group and other laboratories is not possible. Based on our results, a general guideline can be established for screening the existence of excited-state absorption from known linear absorption and fluorescence spectra, thereby alleviating the need to perform excited-state absorption experiments for each crystal.

Ce^{3+} ions doped in A_2BYF_6 (A = Cs or Rb and B = Na or K) crystals possess low excited-state absorption, broad fluorescence bands in the blue-green, and pump bands easily accessible with N_2 or XeCl lasers. Purification and growth procedures for synthesizing single crystals of Cs_2KYF_6 and Kb_2KYF_6 doped with 0.01% Ce^{3+} ions are presented.

Preliminary results on instantaneous two-dimensional concentration mapping of the large-scale coherent turbulent structures from an axisymmetric jet are reviewed. The Rayleigh scattering from the nozzle gas itself and the fluorescence scattering from I_2 molecules seeded in the nozzle gas appear to be viable new optical techniques for turbulence diagnostic studies. The merits of the Rayleigh and fluorescence techniques are compared to those of the Raman (from the nozzle gas itself) and Lorenz/Mie (from aerosols seeded in the nozzle gas) techniques.

Introduction

The first three years of the four-year research period were devoted to the study of the excited-state absorption (ESA) spectroscopy of rare-earth crystals which have the potential of providing a broadly tunable solid-state laser in the blue-green region of the visible spectrum. During the last year of research, the objectives were twofold: (1) to attempt to grow single crystals of Rb_2NaYF_6 doped with 0.1% Ce^{3+} which, based on our previous year's results, showed the best potential of providing tunable laser radiation in the 4000-5000 Å region; and (2) to investigate the viability of Rayleigh scattering from the nozzle gas itself and of fluorescence from I_2 molecules seeded in the nozzle as techniques to map the instantaneous two-dimensional concentration field in turbulent jets. Results of the ESA investigation will be reviewed briefly in this report, as well as our novel approach to growing single crystals of Rb_2NaYF_6 doped with 0.1% Ce^{3+}. The successful results on turbulence field mapping with Rayleigh scattering from the nozzle gas itself and the preliminary results on the use of fluorescence from I_2 molecules seeded in a turbulent jet also will be summarized.

Results in Rare-Earth Crystal Spectroscopy and Growth

Based on linear optical spectroscopy results (e.g., absorption, fluorescence efficiency, and fluorescence lifetime), the broadband 5d → 4f emissions in a number of Eu^{2+} and Ce^{3+} ions doped in metal fluorides, chlorides, fluorochlorides, and garnets appeared to have the potential of

providing broadly tunable laser radiation in the blue-green region of the visible spectrum. We did not succeed in achieving laser action from Eu^{2+} ions doped in CaF_2, BaF_2, SrF_2, $CaCl_2$, $BaCl_2$, $SrCl_2$, BaClF, and SrClF crystals even though their fluorescence parameters appeared to be promising for laser emission (see Appendix A). Furthermore, we did not achieve laser action from Ce^{3+} ions doped in CaF_2, BaF_2, SrF_2, and LaF_3 (see Appendix B). Two other research groups also reported their failures to achieve laser action from Ce^{3+} doped in YAG crystals.[1,2] However, laser emission was reported from Ce^{3+} doped in YLF crystals.[3] Faced with these rather perplexing and seemingly conflicting results in which certain promising crystals can be made to lase while other crystals cannot achieve lasing thresholds, we realized that ESA must be an important parameter, i.e., the optical loss mechanism caused by ESA must be taken into account in the laser threshold equations along with all the usual linear optical parameters. By the end of our second year of work, we concluded that candidate crystals must be characterized by their ESA properties, as well as by the usual linear absorption and fluorescence parameters.

During the third year, we concentrated on ESA studies in Eu^{2+} ions doped in CaF_2 and Ce^{3+} ions doped in YAG. ESA measurements were made at both room temperature and 77°K. For these crystals, the ESA at the lasing wavelengths was caused when the conduction band of the host crystals (CaF_2 and YAG) were too near the rare-earth energy levels which can be populated by the pump radiation. Consequently, the photon energies of the fluorescent radiation caused optical transition from the upper laser level of the Eu^{2+} or Ce^{3+} ions to the conduction band of the host crystal. No

obvious way exists to overcome such ESA occurring at the fluorescent wavelength. In fact, ESA will increase proportionally with pump energy; thus when ESA exists, there is no way to achieve more optical gain by increasing the pump energy. Apparently, for the case of Ce^{3+} doped in YLF, the conduction band is sufficiently removed from the upper laser level compared to the photon energy of the fluorescent radiation. Laser action at 325 nm was achieved by the Lincoln Laboratory group for Ce^{3+} doped in YLF.[3] Consequently, the fact that laser emission for Ce^{3+} ions is achievable in YLF, and not in YAG, CaF_2, BaF_2, SrF_2, and LaF_3, clearly demonstrates that even a small amount of ESA at the fluorescent wavelength is extremely detrimental for laser action.

Based on our ESA results, we were able to develop a general rule, i.e., if the sum of the fluorescence photon energy plus the zero-phonon fluorescence photon energy lies within the linear absorption spectrum, then ESA can exist. Using a combination of the linear absorption spectra to locate the conduction band of the host crystal and of the fluorescence spectra to locate the upper laser levels of the rare-earth ions, the presence of ESA at the fluorescent wavelength can be predicted. This general rule is a valuable guide because, in general, absorption and fluorescence data are available in the literature while ESA spectra are usually unavailable and rather difficult to measure.

In our search for suitable crystal hosts for Ce^{3+} ions, two groups of crystals, A_2BYF_6 and A_2BYCl_6 (where A = Cs or Rb and B = Na or K), appeared to be promising because of their properties: (1) no measurable ESA; (2) broad fluorescence linewidth; (3) reasonably long fluorescence

lifetime; and (4) fluorescence peak centered in the visible portion of the EM spectrum. Figures 1 and 2 show the fluorescence and excitation spectra for Ce^{3+} in Cs_2NaYCl_6 and Cs_2NaYF_6, respectively.

The chloride crystals (Cs_2NaYCl_6) were found to be extremely sensitive to ambient moisture and the crystals with or without Ce^{3+} ions turned brown in appearance under intense pump energy (at λ_{pump} = 3371 Å from a N_2 laser). The exact cause of such photoinduced coloration was not explored further, even though stimulated optical gain (rather than stimulated loss due to ESA) was indeed observed at 4000 Å near the peak of the fluorescence emission (see Fig. 1).

ESA, excitation spectra, and fluorescence spectra in the polycrystalline form of Cs_2NaYF_6 were also investigated. This crystal was found to be quite resistant to ambient moisture and did not cause any brown coloration under intense radiation at λ_{pump} = 3371 Å from a N_2 laser. Stimulated optical gain at the fluorescent wavelength (at 4000 Å) was also observed. However, because of the polycrystalline nature of the sample, which caused a significant amount of scattering, no quantitative measurements of the optical gain were made. We concluded that Ce^{3+} ions in Cs_2NaYF_6 have the following desirable characteristics: (1) fluorescent emission is broad and centered around 4500 Å; (2) pump bands are compatible to the N_2 laser output at 3371 Å or that of the excimer laser XeCl at 3080 Å; (3) the crystal is resistant to the intense UV pump radiation; and (4) the crystal surface seems to be less susceptible to moisture damage than that of Cs_2NaYCl_6.

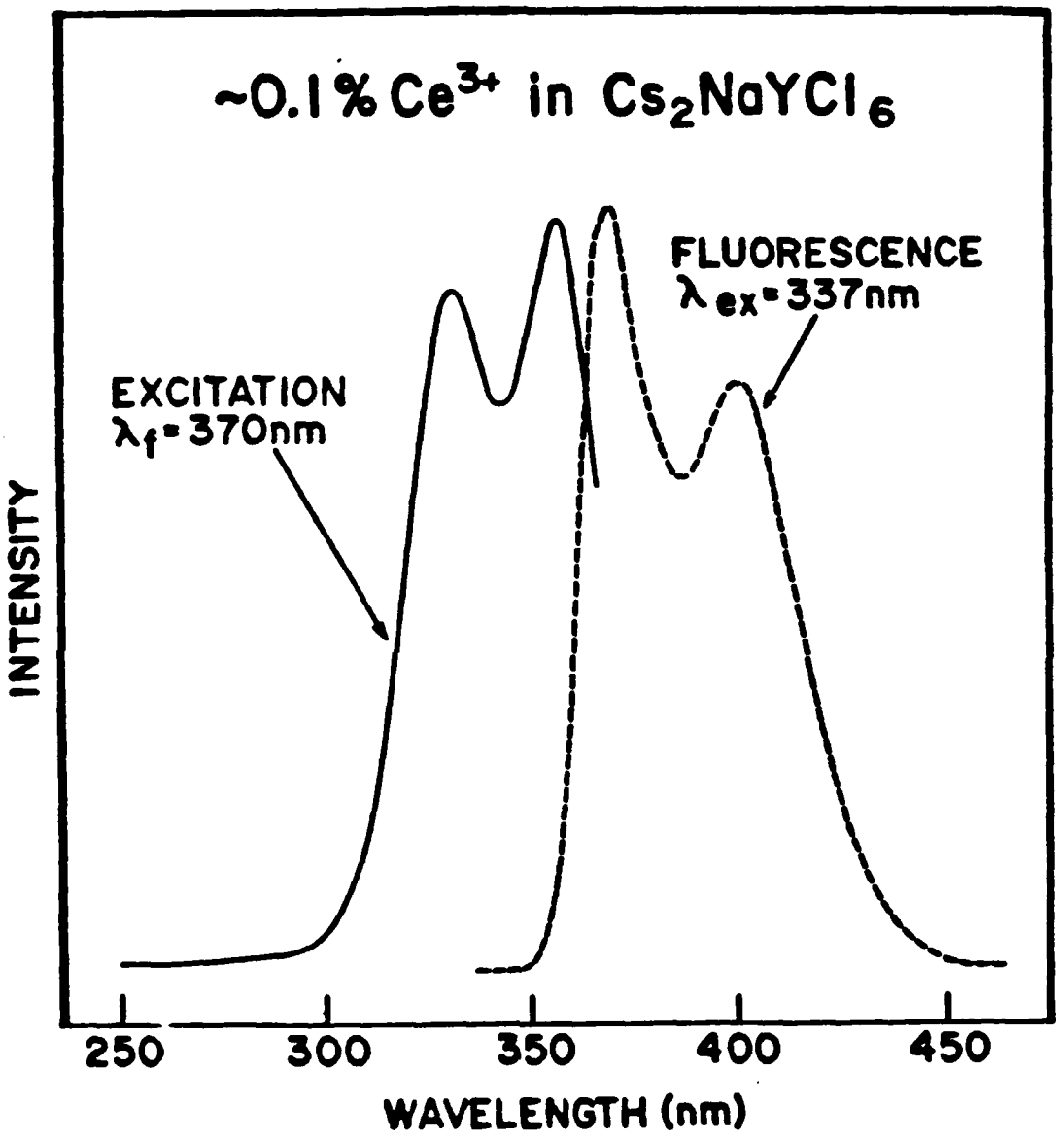

Figure 1. The fluorescence and excitation spectra of $Ce^{3+}:Cs_2NaYCl_6$. To excite the fluorescence, the excitation wavelength was set at 337 nm. The excitation spectra were determined with the fluorescence wavelength λ_f set at 370 nm.

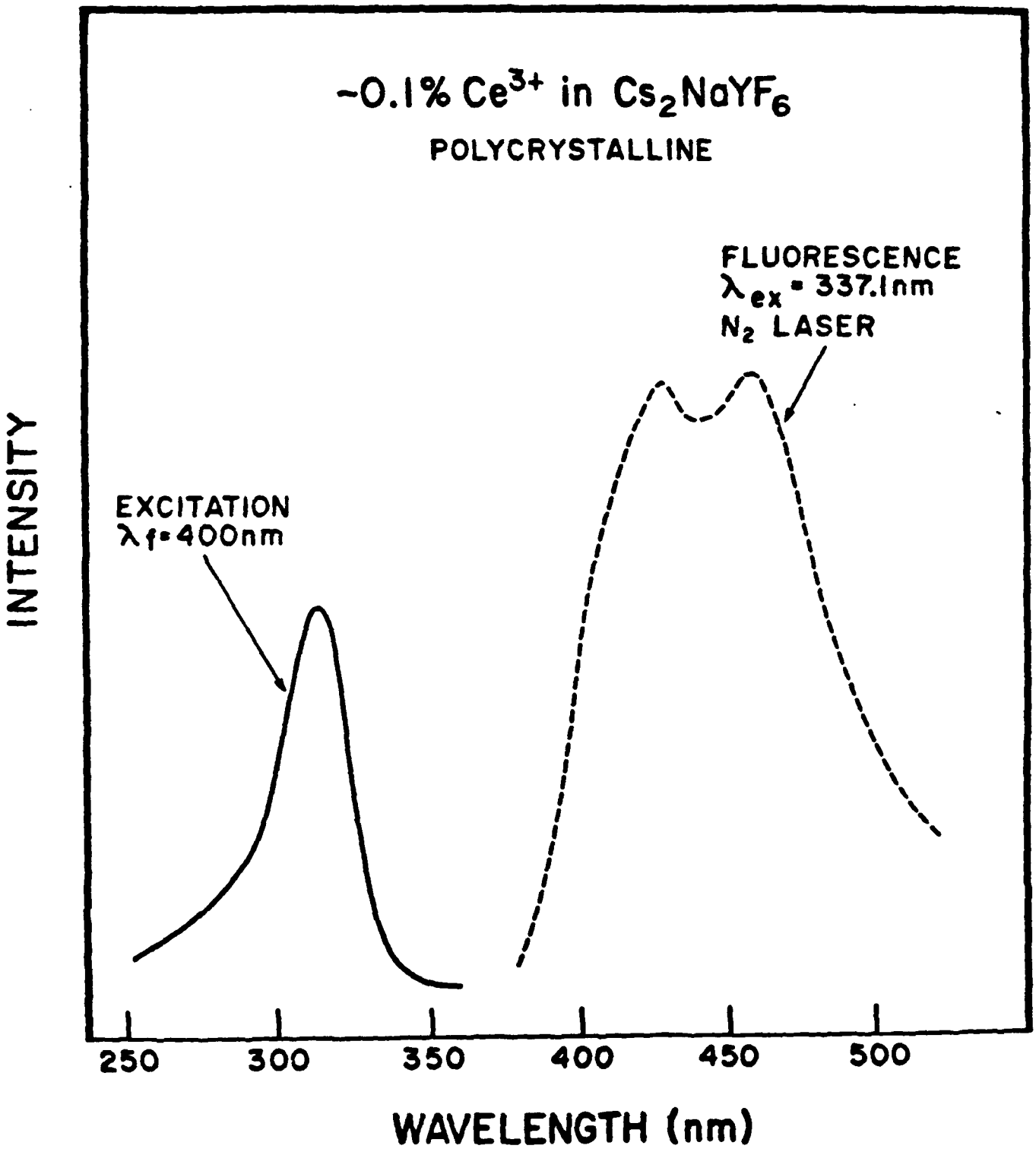

Figure 2. The fluorescence and excitation spectra of Ce^{3+}:Cs_2NaYF_6. A N_2 laser (λ_{ex} = 337.1 nm) excited the crystal, and the resultant fluorescence spectra are shown. The excitation spectra were determined with the fluorescence wavelength λ_f set at 400 nm.

Encouraged by these characteristics, we attempted to grow large single crystals of Cs_2NaYF_6 and Rb_2NaYF_6 containing 0.1% Ce^{3+}. To obtain laser quality single crystals, we realized the importance of chemical purity of the starting material. The purification of starting material involved several steps: (1) wet chemistry to precipitate the undesired ion impurities: (2) low temperature hydrofluorination to eliminate OH^- inclusion; (3) after CeF_3 is added, high temperature fluorination to cause a solid-state reaction and sintering of the mixed chemicals; and (4) chemical cleaning of the manually selected sintered sample. A modified zone refining technique was used to grow small single crystals. See Fig. 3 for a flow chart of the purification and growth procedures.

The sintered material was placed in a Pt boat with HF as the solvent. The Pt boat was then sealed in an inert atmosphere (argon gas) and inserted in a RF zone-refining apparatus. A molten zone of approximately 10% of the boat length was created and made to traverse the entire length of the boat at 3-5 mm per hour. At the two ends of the boat, a mixed phase of fluorides existed, while a small single-phase of clear crystal containing about 0.1% Ce^{3+} ions was produced around the center of the boat. Even though the AFOSR grant has ended, we will continue to attempt to improve the purification and modified RF zone-refining procedures in order to grow larger single crystals of Cs_2NaYF_6, Rb_2NaYF_6, and Rb_2KYF_6 containing $\sim$0.1% Ce^{3+} ions. Once a crystal of reasonable size has been obtained, our efforts to achieve tunable laser action from these fluoride crystals will be resumed.

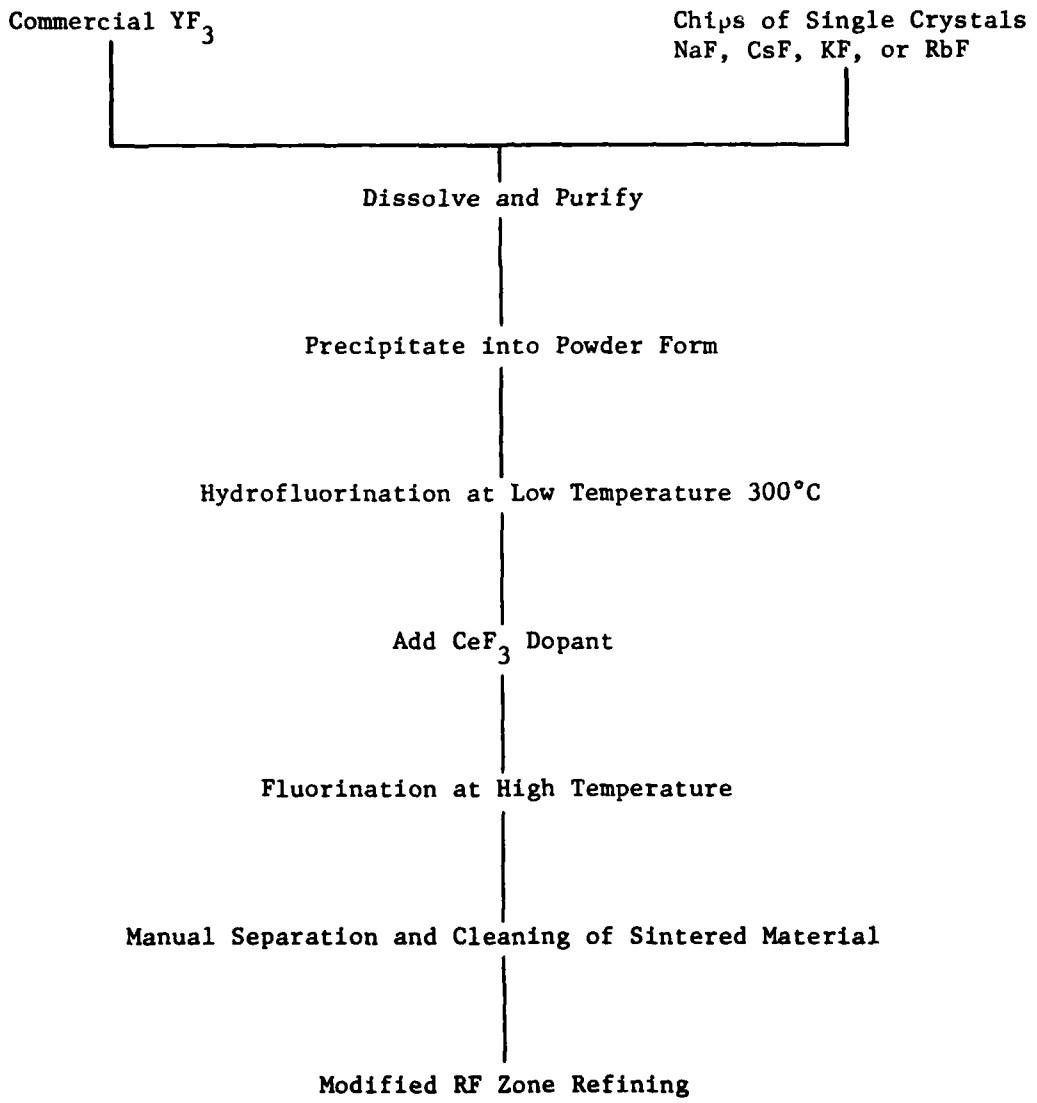

Figure 3. Flow chart of purification and crystal growth procedure.

Results in Concentration Mapping of Turbulent Jets

Under the ONR Project SQUID program, we have developed an instantaneous, two-dimensional, quantitative (in digital form on magnetic tapes) technique to map the concentration field in a turbulent jet. The nozzle gas was seeded with aerosols of less than 0.1 μm in diameter and the Lorenz/Mie scattered light resulting from a sheet of laser radiation, intersecting and made parallel to the jet axis, was recorded with a computer-controlled low-light-level TV camera (PAR OMA-2). The intensity of scattered light is proportional to the number of aerosols which, in turn, are assumed to be representative of the nozzle fluid concentration. Results from the Lorenz/Mie technique provide a wealth of statistical information, e.g., the spatial covariance of the concentration fluctuation within the two-dimensional sheet covering a downstream distance of 6-8 nozzle diameters and the entire jet extent in the radial direction. Our results on the turbulent eddies and their relation to the large vortical structures developed further upstream in the transition region of a jet have been published.[4,5]

The Lorenz/Mie technique has serious limitations, which are summarized as follows: (1) marker shot noise caused by the superlinear dependence of the scattered intensity on the aerosol diameter introduces intensity noise in the concentration field; (2) poor spatial resolution due to the finite number of larger aerosols per unit resolution volume limits this technique to large-scale structure studies; and (3) no molecular diffusion effects due to the large mass ratio between the aerosols and the nozzle gas.

During the last year of the AFOSR research, we explored two possible alternatives to Lorenz/Mie scattering. Both Rayleigh scattering from the nozzle gas itself and fluorescence scattering from I_2 molecules introduced into the nozzle gas were studied as means of overcoming the marker shot noise, poor spatial resolution, and the lack of molecular diffusion peculiar to the aerosols used as tags in the Lorenz/Mie technique.

The elimination of marker shot noise, significant improvement in the spatial resolution, and importance of molecular diffusion effects make the Rayleigh technique considerably more attractive than the former Lorenz/Mie approach. However, the scattering efficiency for Rayleigh scattering is some 10^4 - 10^6 times weaker than that for Lorenz/Mie scattering. A high energy pulsed laser must therefore be used instead of the more convenient cw laser and electronic gating of the TV camera employed for the Lorenz/Mie experiments. Since the Rayleigh scattering intensity is proportional to the square of the refractive index difference between the nozzle gas and its surrounding, the Rayleigh approach places a restriction on the nozzle gas density, i.e., the nozzle gas must be either more dense or less dense than the surrounding medium, e.g., freon-12 or He gas exiting into an ambient environment. Details on the advantages of the Rayleigh scattering and our preliminary results can be found in Appendix C.

Fluorescence scattering from I_2 molecules seeded into the nozzle gas can eliminate the gas density restriction imposed by the Rayleigh technique. Furthermore, since the peak of the I_2 fluorescence spectrum is quite removed from the peak of the absorption spectrum, there is little difficulty in spectrally isolating the elastic scattering (Rayleigh) from the

inelastic I_2 fluorescence emission. Ordinary color glass filters can be used. Consequently, the fluorescence technique is ideally suited for the study of wall jets and other configurations which would give rise to a considerable amount of elastic scattering occurring from boundary interfaces. Thus, for boundary-layer flow studies, even the Lorenz/Mie approach and certainly the Rayleigh scattering technique would be totally inadequate because the elastic scattering from the interface overwhelms the much weaker scattering intensities from the aerosols or nozzle gas molecules.

Instantaneous concentration mapping of an axisymmetric jet with the fluorescence radiation from I_2 molecules was attempted with a small Q-switched Nd:YAG laser, optically doubled to produce 4 mJ of 5320 Å radiation with 20 nsec pulse duration. The I_2 molecules were introduced into the nozzle gas by placing small pellets of I_2 crystals in the gas line supplying the nozzle gas. At room temperature, the vapor pressure of I_2 is about 1 Torr or approximately 10^{16} molecules per cm^3, many orders of magnitude more than the aerosol seeding density used in the Lorenz/Mie technique. However, the fluorescence intensity from I_2, although I_2 is one of the strongest fluorescers, is still very weak compared to the elastic intensity from aerosols. In fact, the I_2 fluorescence intensity is comparable to the Rayleigh intensity from freon-12 gas used in the results reported in Appendix C. The instantaneous one-shot results are shown in Fig. 4. Note the low-signal-to-noise ratio and the presence of large intensity spikes caused by the optical leakage through the color filters of the elastic scattering from spurious aerosols

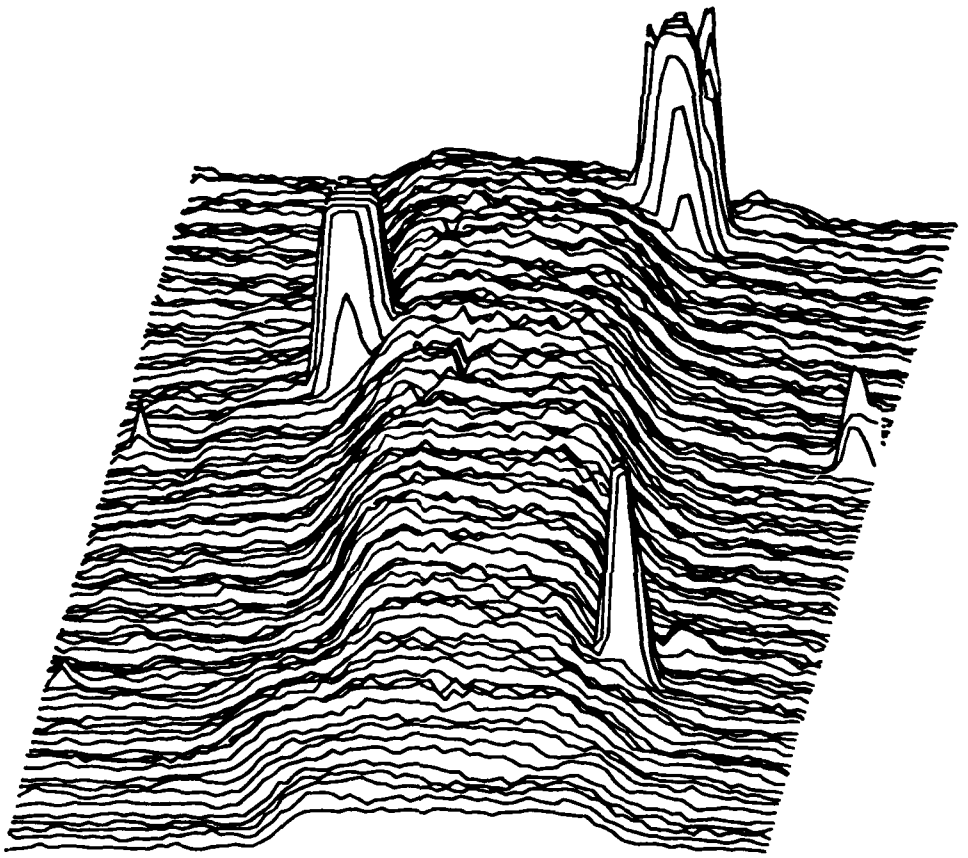

Figure 4. Instantaneous two-dimensional profile of I_2 fluorescence. The I_2 molecules are seeded in the nozzle gas. The incident laser beam is focused into a sheet of radiation parallel to the axis of an axisymmetric jet. The fluorescence radiation is collected normal to the illumination plane, optically isolated from the incident laser wavelength by colored filters, and detected with a low-light-level television camera.

floating around in the testing chambers. We believe that the I_2 fluorescence technique can definitely be useful if the incident laser energy is increased to 40-100 mJ per pulse.

Based on our preliminary results shown in Fig. 4, we intend to use a commercially available laser to provide some 100-200 mJ per pulse and to apply the I_2 fluorescence mapping technique to study wall jets. Now that we have made the intensity comparisons for Lorenz/Mie, Rayleigh, I_2 fluorescence, and Raman scattering techniques, as well as evaluated the advantages and disadvantages of these four approaches, we will continue to exploit the various merits of each in terms of the physical parameters being measured in turbulent flows.

The Raman scattering technique undoubtedly provides the greatest amount of information, particularly under a combustion situation, since the Raman spectra are unique to the molecular species. However, the weak Raman scattering efficiency requires extremely large input laser energies which are not available except from lasers being operated by national laboratories.

Our results from both the Rayleigh and I_2 fluorescence techniques are very encouraging. These two alternative approaches to concentration mapping will enable us and others to study small scale turbulent structures (e.g., the Kolmognov scales) and the thickness of superlayers. For many cold flow turbulence studies, the Rayleigh and/or fluorescence techniques appear to be far more viable than the Raman technique.

References

1. R. R. Jacobs, William F. Krupke, and Marvin J. Weber, "Measurement of Excited-State Absorption Loss for Ce^{3+} in $Y_3Al_5O_{12}$ and Implications for Tunable 5d→4f Rare-Earth Lasers," Appl. Phys. Lett. 33, 410 (1978).
2. W. J. Miniscalo, J. M. Pellegrino, and W. M. Yen, "Measurements of Excited-State Absorption in Ce^{3+}:YAG," J. Appl. Phys. 49, 6109 (1978).
3. D. J. Ehrlich, P. F. Moulton, and R. M. Osgood, Jr., "Ultraviolet Solid-State Ce:YLF Laser at 325 nm," Opt. Lett. 4, 184 (1979).
4. M. B. Long, B. T. Chu, and R. K. Chang, "Instantaneous Two-Dimensional Gas Concentration Measurements by Light Scattering," AIAA Journal 19, 1151 (1981).
5. M. B. Long and B. T. Chu, "Mixing Mechanism and Structure of an Axisymmetric Turbulent Mixing Layer," AIAA Journal 19, 1158 (1981).

Publications

1. Takao Kobayasi, Stanley Mroczkowski, James F. Owen, and Lothar H. Brixner, "Fluorescence Lifetime and Quantum Efficiency for 5d → 4f Transitions in Eu^{2+} Doped Chloride and Fluoride Crystals," J. Lumin. 21, 247 (1980). [Appendix A]
2. James F. Owen, Paul B. Dorain, and Takao Kobayasi, "Excited-State Absorption in Eu^{+2}:CaF_2 and Ce^{+3}:YAG Single Crystals at 298° and 77°K," J. Appl. Phys. 52, 1216 (1981). [Appendix B]
3. M. Carla Escoda and Marshall B. Long, "Rayleigh Scattering Measurements of the Gas Concentration Field in Turbulent Jets," (submitted to AIAA). [Appendix C]
4. H. M. Tzeng and Marshall B. Long, "Gas Concentration Field Mapping with Fluorescence from I_2 Seeded in Turbulent Jets," (to be submitted to AIAA Journal).

Personnel

In addition to the Principal Investigator, the following people have participated in this research project:

Takao Kobayasi	-	Visiting Scientist from the Research Institute of Electrical Communications, Tohoku University, Sendai, Japan.
Paul B. Dorain	-	Visiting Professor from the Department of Chemistry, Brandeis University, Waltham, MA.
James F. Owen	-	Assistant Professor of Applied Physics.
Stanley Mroczkowski	-	Senior Research Associate and Lecturer in Applied Physics.
Lothar H. Brixner	-	Collaborator from E. I. du Pont de Nemours & Company, Central Research and Development Department, Experimental Station, Wilmington, DE.
Marshall B. Long	-	Assistant Professor of Applied Mechanics.
M. Carla Escoda	-	Graduate student.
Vitali Korobov	-	Graduate student.
Daniel Murphy	-	Graduate student.
Huey-Ming Tzeng	-	Graduate student.
Mark Havstad	-	Undergraduate student.
Daniel Shepard	-	Undergraduate student.

APPENDIX A

Journal of Luminescence 21 (1980) 247–257

FLUORESCENCE LIFETIME AND QUANTUM EFFICIENCY FOR 5d → 4f TRANSITIONS IN Eu^{2+} DOPED CHLORIDE AND FLUORIDE CRYSTALS*

Takao KOBAYASI **, Stanley MROCZKOWSKI and James F. OWEN
Department of Engineering and Applied Science, Yale University, New Haven, CT 06520, USA

and

Lothar H. BRIXNER
E.I. du Pont de Nemours and Company, Central Research and Development Department, Experimental Station, Wilmington, DE 19898, USA

Received 19 October 1979

An investigation of the relevant parameters for broadly tunable lasers utilizing the efficient, broad-band 5d → 4f emission in a number of Eu^{2+} doped metal fluorides, chlorides, and fluoro-chlorides has been performed. Results of measurements of absorption and emission spectra, quantum efficiencies, and fluorescence lifetimes in MF_2 and MCl_2 (M = Ca, Ba, Sr) and MFCl (M = Ba, Sr) are presented. A calculation of the pump energy threshold for laser action in CaF_2 : Eu^{2+} based on our spectroscopic data is made. Although the estimation indicated that laser threshold in CaF_2 : Eu can be easily achieved, strong excited-state absorption in this system was found to prohibit laser oscillation.

1. Introduction

The strong, broad-band fluorescence emission, resulting from 5d → 4f transitions, exhibited by divalent and trivalent rare-earth ions in a large number of host crystals makes many of these systems likely candidates for the active media of broadly tunable solid state lasers [1–4]. Because the 5d orbitals of the rare-earth ions interact strongly with the crystal lattice, the electric dipole transitions from the 4f ground state to the 5d states give rise to broad absorption bands. In cases where the crystal field brings the lowest 5d level below the first excited 4f state, broad-band emission with large Stokes shifts occurs. These absorption and emission characteristics are similar to those of the active media of a number of broadly tunable solid state lasers. For example, alkali halides containing color centers [5], and various

* Supported in part by AFOSR Grant No. 77-3433.
** Present address: Research Institute of Electrical Communication, Tohoku University, Sendai, Japan.

hosts containing transition metal ions, such as Ni^{2+} in MgF_2 [6] and Cr^{3+} in Al_2BeO_4 [7], give rise to phonon broadened emission in the red and infrared spectral regions and have been used successfully in laser applications. Very recently, laser action, tunable over 20 to 30 nm near 325 nm, has been achieved in Ce^{3+} doped $LiYF_4$ pumped at 249 nm with a KrF laser [8].

Since Eu^{2+} exhibits efficient 5d → 4f emission in a great number of hosts, with wavelength ranges that virtually cover the visible and near ultraviolet (390–640 nm), an investigation of the optical parameters relevant for possible laser action in Eu^{2+} doped compounds is warranted. Such compounds have been studied extensively as essential components of phosphors for fluorescent lamps and medical X-ray intensifying screen applications [9]. In this paper we report measurements of the absorption and emission spectra, quantum efficiencies, and fluorescence lifetimes of Eu^{2+}: 5d → 4f and 4f → 4f transitions in various chlorides, MCl_2 (M = Ca, Sr, Ba), fluorides, MF_2 (M = Ca, Sr, Ba), and fluoro-chlorides, MFCl (M = Sr, Ba). Although the absorption and fluorescence spectra of most of these compounds have been measured previously [9–15], few accurate values of quantum efficiencies and fluorescence lifetimes are available. Laser threshold calculations are presented, and the feasibility of laser operation is discussed. In addition, we have performed a preliminary investigation on the excited-state absorption in $CaF_2 : Eu^{2+}$ which indicates that laser action in this system is thwarted by strong absorption from the lower excited 5d level to higher lying states [16]. These results are similar to those recently observed in YAG : Ce^{3+} [3,4].

2. Experimental techniques

2.1. Sample preparation

The chloride single crystals doped with Eu^{2+} ions, $MCl_2 : Eu^{2+}$ (M = Ca, Sr, Ba), used in this work were prepared by the Bridgman technique. Fluoro-chloride mixed crystals, MFCl : Eu^{2+} (M = Sr, Ba), were pulled from melt using the Czochralski method. Details of the crystal preparation can be found elsewhere [17]. The fluoride samples, single crystals of CaF_2, SrF_2, and BaF_2 doped with Eu^{2+}, were grown by Optovac. Standard mechanical polishing techniques utilizing alumina polishing abrasives were used to prepare crystal surfaces for optical measurements.

2.2. Optical measurements

Measurements of absorption spectra were performed on a Beckman model DK-2A spectrophotometer. Emission spectra were obtained using a Jarrel–Ash ¼ m monochromator, having a spectral resolution of 0.5 nm, with an EMI 9635QD ultraviolet-sensitive photomultiplier. The spectral response of the detection system was calibrated with a standard tungsten-iodine vapor lamp (3200 K color tempera-

ture). The excitation source for the emission measurements was provided by either a low-pressure Hg lamp with a series of optical filters or a Xe lamp followed by a monochromator.

The quantum efficiencies were determined by comparing the fluorescence intensity of the polished single crystals with that from a standard sample of known quantum efficiency under identical experimental conditions. The value of the quantum efficiency of the crystal is then given by

$$\eta = \eta_{st}(\lambda)(F/F_{st})\, n_{st}/n\,, \tag{1}$$

where $\eta_{st}(\lambda)$ is the absolute quantum efficiency of the standard at wavelength λ, F and F_{st} are the relative integrated fluorescence intensities, and n and n_{st} are the number of pump photons per second absorbed by the crystal and the standard, respectively. For this work sample dopings were such that the total pump radiation was absorbed within a few millimeters of the surface and the fluorescence was collected in the backwards direction. The same was true for the standard sample, thus making $n_{st}/n = 1$. POPOP dye in cyclohexane was chosen as the reference standard because of its spectral similarity to the Eu^{2+} compounds. Care was taken to avoid concentration quenching in the POPOP sample.

For the measurements of fluorescence lifetimes a nitrogen laser, which produced 5 ns pulses at 337.1 nm with 600 kW peak power, was used as the excitation source. The decay rate was obtained from oscilloscope traces. The overall response time of the detection system was 30 ns.

For the investigation of excited-state absorption in $CaF_2 : Eu^{2+}$ the beam from the nitrogen laser was split, half of the beam being used to pump the crystal directly, the other half being used to pump a dye laser which served as the probe beam. Transmission of the probe beam through the sample was detected with a photodiode preceded by a monochromator which reduced the broad-band fluorescence from the crystal and passed the probe beam wavelength. The pump beam, directed almost collinearly with the probe beam, was focused on the face of the sample at the point at which the probe beam entered the crystal. Sample doping was such that the pump beam was totally absorbed within 1 mm of the surface. The excited-state absorption was determined by comparing the transmission of the probe beam through the sample with and without irradiation of the sample by the pump beam.

3. Results

The absorption spectra for Eu^{2+} in $SrCl_2$ and $BaCl_2$ and the relative fluorescence spectra for Eu^{2+} in $CaCl_2$, $SrCl_2$ and $BaCl_2$, measured at room temperature, are shown in fig. 1. The excitation wavelength for the fluorescence is 365 nm. At this wavelength the penetration depth is less than 1 mm for all the samples. The emission spectra, which result from $5d \rightarrow 4f$ transitions, agree well with previously published data [14]. The fluorescence spectra of the three samples are quite similar

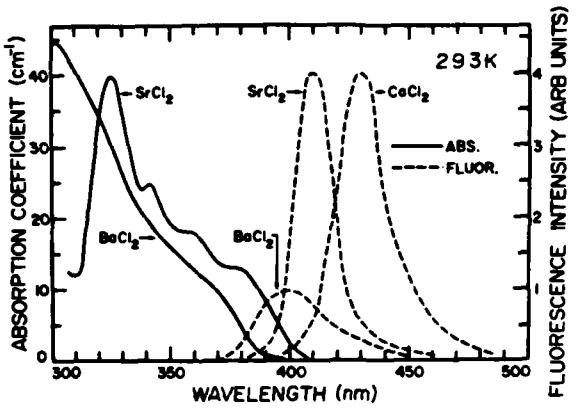

Fig. 1. Absorption spectra of Eu^{2+} doped $BaCl_2$ and $SrCl_2$ (solid lines); emission spectra of Eu^{2+} doped $BaCl_2$, $SrCl_2$ and $CaCl_2$ (dashed lines).

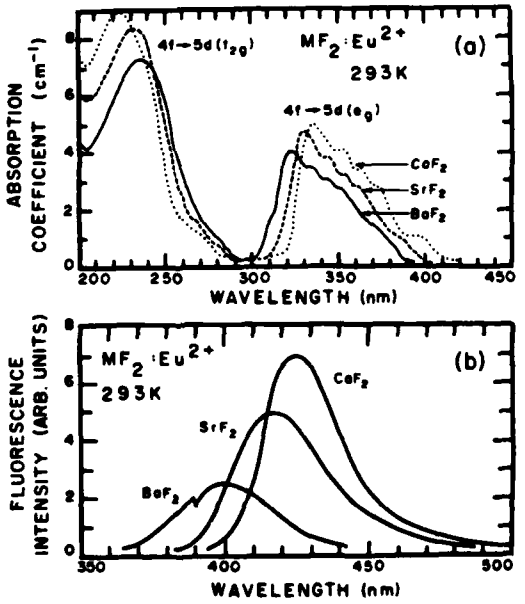

Fig. 2. The 4f → 5d absorption spectra (a) and 5d → 4f fluorescence spectra (b) of Eu^{2+} in MF_2 (M = Ba, Sr, Ca) at room temperature. The nominal Eu^{2+} concentrations in MF_2 (M = Ba, Sr and Ca) are 0.1, 0.2, 0.6 mol%, respectively.

except for a change in the halfwidths and a shift in the peak wavelengths. The emission is particularly intense for both $SrCl_2 : Eu^{2+}$ and $CaCl_2 : Eu^{2+}$.

The room temperature absorption and fluorescence spectra of Eu^{2+} in CaF_2, SrF_2 and BaF_2 are shown in fig. 2. In fig. 2a two strong absorption bands are observed, the higher energy band resulting from the $4f \rightarrow 5d$ (t_{2g}) transitions and the lower energy bands from the $4f \rightarrow 5d$ (e_g) transitions [9]. The fluorescence spectra of these systems are compared in fig. 2b. Again the excitation wavelength is 365 nm and is absorbed close to the sample surface. The $5d \rightarrow 4f$ fluorescence in $BaF_2 : Eu^{2+}$ was observed, to our knowledge, for the first time. Its fluorescence is very weak at room temperature but increases slightly at liquid nitrogen temperature.

Because the 5d electrons interact strongly with the lattice, the location of the 5d energy bands depends upon the symmetry and size of the cation site in the host lattice. The symmetries of the various chloride compounds are different: orthorhombic Pnnm for $CaCl_2$, cubic Fm3m for $SrCl_2$, and orthorhombic Pnam for $BaCl_2$, while all three fluorides have cubic Fm3m symmetry. The systematic energy shifts of the absorption and fluorescence bands in these systems have been ascribed to the change in size and change in electropositivity of the cation of the host and resultant change in the host crystal band gap [9].

Emission resulting from $5d \rightarrow 4f$ transitions also occurs in some Eu^{2+} doped fluoro-chloride compounds [9,18]. The fluorescence spectra for $SrFCl : Eu^{2+}$ (2.0%) and $BaFCl : Eu^{2+}$ (1.0%) are shown in fig. 3. At room temperature these compounds exhibit broad and strong fluorescence resulting from the $5d \rightarrow 4f$ transitions as well as sharp line emission which has been assigned to $4f\,(^6P_{7/2}) \rightarrow 4f\,(^8S_{7/2})$ transitions [18]. The presence of both $5d \rightarrow 4f$ and $4f \rightarrow 4f$ transitions indicates the proximity of the lowest excited 5d and the $4f^7(^6P_{7/2})$ levels. A schematic configuration coordinate diagram of Eu^{2+}, in which only the lowest excited 5d and $4f^7(^6P_{7/2})$ levels are included, is shown in fig. 4. The relative positions of the 5d and $^6P_{7/2}$ levels change in different hosts. Strong $5d \rightarrow 4f$ band emission occurs when the 5d level is significantly lower than the $^6P_{7/2}$ level, $4f \rightarrow 4f$ line emission appears when the reverse is true, and both $5d \rightarrow 4f$ and $4f \rightarrow 4f$ transitions occur when the energy levels are close together.

The relative intensities of the line and band emission are also a function of temperature [18,19]. Included in fig. 3 are the emission spectra of the fluoro-chlorides at liquid nitrogen temperature. At 77 K a great enhancement of the $4f \rightarrow 4f$ lines and a corresponding reduction of the $5d \rightarrow 4f$ fluorescence are observed. This can be explained by assuming that the 5d level lies slightly above the 4f level. At room temperature the 5d level is thermally populated by the 4f level, which has a very long optical lifetime relative to the 5d states, giving rise to the strong $5d \rightarrow 4f$ fluorescence. At 77 K thermal population of the 5d state is greatly reduced; thus, optical transitions take place primarily from the $4f\,(^6P_{7/2})$ level. From an analysis of the relative intensities of the $4f \rightarrow 4f$ line and $5d \rightarrow 4f$ band emission as a function of temperature Sommerdijk et al. [19] have determined that the energy difference between the excited 5d and 4f levels is 0.060 eV in SrFCl and 0.050 eV in BaFCl.

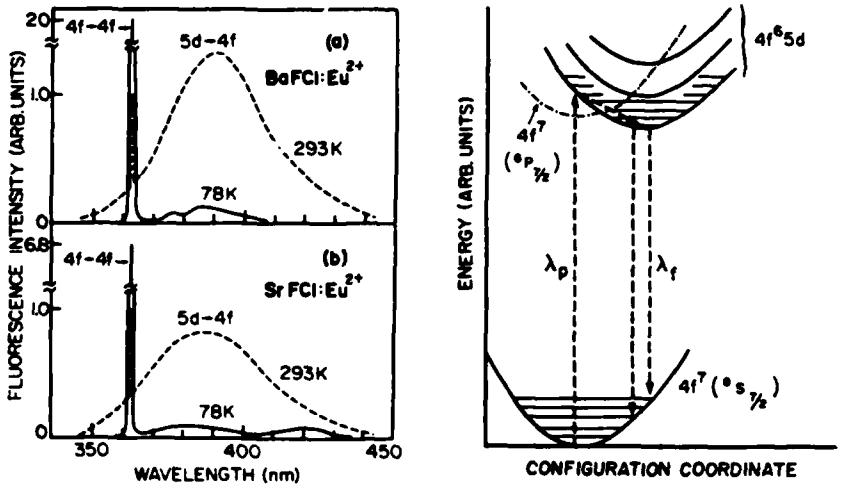

Fig. 3. The fluorescence spectra for BaFCl : Eu^{2+} (1.0 mol%) (a) and SrFCl : Eu^{2+} (2.0 mol%) (b), compared at room temperature (dashed lines) and liquid nitrogen temperature (solid lines).

Fig. 4. Schematic configuration diagram of Eu^{2+} in crystals. Stark splitting and higher excited levels are not shown.

Table 1 summarizes the observed values of the fluorescence peak wavelengths λ_f, halfwidths $\Delta\lambda$, and quantum efficiencies η, at both room temperature and liquid nitrogen temperature. The values in table 1 are averaged results from a number of samples of varying Eu^{2+} concentrations. The range of concentrations is indicated in column 2. The excitation wavelength for all crystals was 365 nm, with the exception of SrFCl and BaFCl for which an excitation wavelength of 253.7 nm from a Hg lamp was used. These wavelengths are well within the 4f → 5d absorption bands. Concentration quenching was not observed in the chloride or fluoride compounds. The variation of η from sample to sample of the same compound was approximately 15%. Also listed in table 1 are the fluorescence lifetimes, τ, measured from radiation emitted near the sample surface. The uncertainty in these values is about 10%. Our measured value of τ for CaF_2 : Eu^{2+} is slightly longer than the reported value of $\tau \approx 0.63$ s [20]. For BaFCl and SrFCl our values of τ for the 5d → 4f transitions at room temperature are larger than those of Sommerdijk et al. by 20 and 400%, respectively.

The fluorescence quantum efficiency for the 5d → 4f transitions can be expressed as

$$\eta = \eta_{nr}\,\eta_r\,, \tag{2}$$

where η_{nr} is the nonradiative energy transfer efficiency for the upper 5d band to

Table 1
Quantum efficiencies, lifetimes and spectral parameters of Eu^{2+} 5d → 4f and 4f → 4f emissions

Host crystal	Eu^{2+} concentration range (mol%)	Temperature (K)	Peak wavelength λ_f (nm)	Halfwidth $\Delta\lambda$ (nm)	Quantum efficiency η	Fluorescence τ (μs)
$BaCl_2$	0.0005–0.1	293	399	33	0.41	0.58
		78	398	22	0.36	0.40
$SrCl_2$	0.005–0.1	293	410	19	0.93	0.95
		78	406	11	0.44	0.70
$CaCl_2$	0.001–0.1	293	430	20	0.97	0.80
		78	427	15	0.87	0.70
BaF_2	0.05–1.0	293	≈403	–	–	–
		78	399	45	<0.01	–
SrF_2	0.05–0.2	293	416	38	0.17	0.55
		78	414	26	0.34	0.75
CaF_2	0.01–0.6	293	424	30	0.62	0.80
		78	420	22	0.62	0.80
BaFCl	1.0–2.0	293	390	37	0.27 [a]	7.0
		>78	385	–	–	–
		293	362 [b]	<0.1	≈0.01 [a]	7.0
		78	362 [b]	<0.1	–	600
SrFCl	2.0	293	387	38	0.20 [a]	5.0
		>78	375	–	–	–
		293	363.5 [b]	<0.1	≈0.01 [a]	5.0
		78	363.5 [b]	<0.1	–	340

[a] Excitation wavelength λ_p = 253.7 nm.
[b] 4f → 4f line.

the bottom of the 5d band and η_r is the radiative ratio or branching ratio of the 5d → 4f transition rate, which is related to the observed fluorescence lifetime τ and the radiative lifetime τ_0 as

$$\eta_r = \tau/\tau_0 \,. \tag{3}$$

For the chloride and fluoride compounds $\eta_{nr} \approx 1$ since the nonradiative lifetime is very fast (<1 ns). Thus, using τ and η in table 1, τ_0 can be calculated from eqs. (2) and (3).

The extremely long lifetimes of the 4f → 4f line emission in BaFCl and SrFCl compounds are characteristic of electric dipole forbidden transitions. The 5d → 4f band emission of these compounds also have rather long lifetimes as compared with other compounds. This is indicative of the mixed electric dipole and magnetic

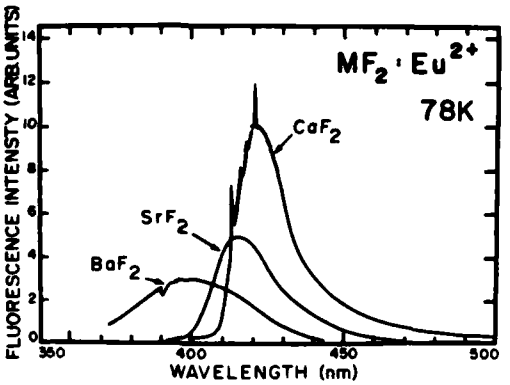

Fig. 5. Fluorescence spectra of $MF_2 : Eu^{2+}$ (M = Ba, Sr and Ca) at liquid nitrogen temperature.

dipole nature of the transitions, consistent with the spectral analysis discussed in ref. [9].

Upon cooling the fluoride and chloride compounds from room temperature to liquid nitrogen temperature, the 5d → 4f fluorescence peaks shift toward shorter wavelengths and the halfwidths narrow without significant change in spectral lineshape. The only exception is $CaF_2 : Eu^{2+}$, where several narrow lines are superimposed on the broad-band emission, as shown in fig. 5. These line spectra are believed to result from the narrowing of the vibrational levels in the 4f ($^8S_{7/2}$) ground state. From a theoretical calculation of the phonon structure and an analysis of the sideband fluorescence of $CaF_2 : Eu^{2+}$, the shortest wavelength peak, at 413 nm, has been identified as the zero phonon line and the peak near 421 nm has been assigned to the transition to the $2\omega_v$ level (two-phonon line) of the E_g phonon mode ($\hbar\omega_v$ = 199 cm^{-1}) [21].

4. Discussion

4.1. Laser threshold estimations

Based on the quantum efficiencies and fluorescence lifetimes obtained in the previous section, an estimate of the possible performance of a Eu^{2+} laser with 5d → 4f transitions can be made. At room temperature the terminal levels (higher vibrational levels of the ground 4f band) are thermally populated and, therefore, Eu^{2+} becomes a three-level laser system. The threshold pump energy density, ρ_{th}, for a three-level system, assuming pulsed operation with the pump pulse duration shorter than the lifetime τ, can be approximated as

$$\rho_{th}^{(3)} = (N/2\eta)(hc/\lambda_p)\,, \qquad (4)$$

where N is the Eu^{2+} ion density and λ_p is the pump wavelength.

At low temperatures the terminal levels are less populated since the number of occupied higher vibrational levels decreases according to the Boltzman relation, $\exp(-n\hbar\omega_v/kT)$, where n is the vibrational quantum number and ω_v is the vibrational frequency in the ground state. In $CaF_2 : Eu^{2+}$, for example, where the peak emission at 421 nm corresponds to the $n = 2$ level and $\hbar\omega_v = 199\ cm^{-1}$, $n\hbar\omega_v << kT$ is achieved at 78 K, and a four-level system can be realized. The pump energy density threshold for a four-level system is given by

$$\rho_{th}^{(4)} = \left(\frac{8\pi^2 \Delta\nu\tau n_r^3}{(\pi \ln 2)^{1/2} c\lambda_f^2 \tau_c \eta}\right)\left(\frac{hc}{\lambda_p}\right) \tag{5}$$

where $\Delta\nu$ is the fluorescence bandwidth, n_r is the refractive index of the crystal, and τ_c is the decay time of the cavity.

Using $CaF_2 : Eu^{2+}$ in a small volume laser scheme (mini-laser) optically pumped by another laser (such as an N_2 or excimer laser) and assuming an active volume $V_p = 1 \times 1 \times 5\ mm^3$, $N = 2.5 \times 10^{19}$ for a Eu^{2+} concentration of 0.1 mol%, and an absorption coefficient $k_p = 10\ cm^{-1}$ at $\lambda_p = 337$ nm, the energy density required to reach lasing threshold in a three-level system is $\rho_{th}^{(3)} = 12\ J\ cm^{-3}$. The actual pump energy required, $E_{th} = \rho_{th} V_p$, is 60 mJ. For a large volume flashlamp pumped laser, if $V_p = 10 \times 10 \times 20\ mm^3$ and $N = 2.5 \times 10^{18}$, then $E_{th} = 2.4$ J. For a four-level laser system, assuming $\tau_c = 3.0$ ns for 10% round trip loss with a 10 cm cavity, $\Delta\nu = 22$ nm, $\tau = 0.8 \times 10^{-6}$ s, $\lambda_f = 420$ nm, and $n_r = 1.5$, the threshold energy density required from the pump source is $\rho_{th}^{(4)} = 33\ mJ\ cm^{-3}$, giving a total energy requirement of $E_{th}^{(4)} = 0.17$ mJ for the mini-laser and 66 mJ for the flashlamp pumped laser. For comparison, Ehrlich et al. [8] experimentally found the lasing threshold for their Ce^{3+} doped $YLiF_4$ mini-laser, a four-level system, to be 0.12 J cm^{-2}, which corresponds to an energy density of about 1.0 J cm^{-3} in their crystal.

The strong line emission of the $4f \rightarrow 4f$ transitions which occur in Eu^{2+} doped BaFCl and SrFCl make these and other similar compounds potential candidates for laser applications. Although the narrow linewidths prohibit broad tunability, the quantum efficiencies are relatively large at low temperatures and the long lifetimes are advantageous for high energy storage laser systems. Even at low temperatures laser threshold calculations for these transitions must be based on a three-level system.

4.2. Excited-state absorption

Since $CaF_2 : Eu^{2+}$ appeared to be one of the more promising of the compounds studied in this work for laser application, an attempt was made to observe laser action in this system. Since laser oscillation did not occur, an investigation of excited-state absorption in $CaF_2 : Eu^{2+}$ was begun. Using the setup described in the previous section, an attenuation of a 420 nm probe beam of almost 50% was observed upon passing through an optically pumped 0.6 mol% Eu^{2+} doped CaF_2 crys-

tal. Only reflection losses were observed with the pump beam blocked from the sample. Thus, it is clear that relatively large excited-state absorption occurring in the emission band thwarts laser action in this system. Preliminary results at room temperature [16] indicate that the excited-state absorption is broad, covering the entire visible region, and may result from transitions from the 5d (e_g) to the 5d (t_{2g}) band, with the selection rules for such transitions being relaxed because of mixing of the upper states and the proximity of the conduction band. Similar results have been observed in Ce^{3+} doped YAG [3,4]. A detailed investigation of excited-state absorption in some of the other Eu^{2+} doped compounds is in progress.

For $CaF_2 : Eu^{2+}$ it was observed that the measured fluorescence lifetime was dependent upon the point in the sample from which the emitted radiation was collected. The lifetime for radiation emitted within the sample was found to be two to three times longer than that for radiation collected from a volume close to the sample surface. Since excited-state absorption gives rise to another mechanism for depopulation of the upper level of the fluorescing transition, the observed fluorescence lifetime in a material exhibiting excited-state absorption will decrease with increasing population of the excited state. The difference between the pump intensity at the surface and within the sample may be responsible for the observed depth dependence of the fluorescence lifetime in $CaF_2 : Eu^{2+}$.

5. Conclusion

We have measured the 5d → 4f fluorescence spectral properties, particularly the quantum efficiencies and lifetimes for Eu^{2+} in various chloride, fluoride, and fluorochloride compounds. The high quantum efficiencies for the chloride and CaF_2 crystals coupled with the broad emission bands make such materials good candidates for tunable lasers.

Because of excited-state absorption in $Eu^{2+} : CaF_2$, laser action in this system could not be achieved. However, since the 5d band energy is very sensitive to lattice parameters, symmetries, and temperature, it may be possible to avoid excited-state absorption in a Eu^{2+} system by selecting the proper host crystals and operating temperatures. These results indicate the value of excited-state absorption measurements in any investigation of materials for broadly tunable laser application.

Acknowledgement

We wish to thank Prof. R.K. Chang for helpful discussions during the course of this work.

References

[1] K.H. Yang and J.A. DeLuca, Appl. Phys. Lett. 29 (1976) 499.
[2] K.H. Yang and J.A. DeLuca, Appl. Phys. Lett. 31 (1977) 594.
[3] R.R. Jacobs, W.F. Krupke and M.J. Weber, Appl. Phys. Lett. 33 (1978) 410.
[4] W.J. Miniscalco, J.M. Pellegrino and W.M. Yen, J. Appl. Phys. 49 (1978) 6109.
[5] L.F. Mollenauer and D.H. Olson, J. Appl. Phys. 46 (1975) 3109.
[6] P.F. Moulton, A. Mooradian and T.B. Reed, Opt. Lett. 3 (1978) 164.
[7] J.C. Walling, H.P. Jenssen, R.C. Morris, E.W. O'Dell and O.G. Peterson, Opt. Lett. 4 (1979) 182.
[8] D.J. Ehrlich, P.F. Moulton and R.M. Osgood, Jr., Opt. Lett. 4 (1979) 184.
[9] L.H. Brixner, J.D. Bierlein and V. Johnson, Current Topics in Material Science, vol. 4, ed. E. Kaldis (North-Holland, Amsterdam, 1980) in press.
[10] F.D.S. Butement, Trans. Faraday Soc. 44 (1948) 617.
[11] S. Freed and S. Katcoff, Physica 14 (1948) 17.
[12] A.A. Kaplyanskii and P.P. Feofilov, J. Opt. Spectrosc. 13 (1962) 129.
[13] G.H. Dieke and H.M. Crosswhite, Appl. Opt. 2 (1963) 675.
[14] L.H. Brixner and A. Ferretti, J. Solid State Chem. 18 (1976) 111.
[15] J.L. Sommerdijk and A.L.N. Stevels, Philips Tech. Rev. 37 (1977) 221.
[16] J.F. Owen, P.B. Dorain, S. Mroczkowski and R.K. Chang, 1979 Annual Meeting, Optical Society of America, Rochester, NY (8–12 Oct. 1979).
[17] S. Mroczkowski, M. Havstad and T. Kobayasi, Abstr. 4th Am. Conf. on Crystal Growth, N.B.S., Maryland (July 1978) p. 88.
[18] B. Tanguy, P. Merle, M. Pezat and C. Fouassier, Mater. Res. Bull. 9 (1974) 831.
[19] J.L. Sommerdijk, J.M.P.J. Verstegen and A. Bril, J. Luminescence 8 (1974) 502.
[20] N.A. Tolstoy, Dokl. Akad. Nauk, SSSR 102 (1955) 935.
[21] Z. Kam and E. Cohen, Solid State Commun. 14 (1974) 1111.

Excited-state absorption in Eu^{+2}: CaF_2 and Ce^{+3}: YAG single crystals at 298 and 77 K

James F. Owen, Paul B. Dorain,[a] and Takao Kobayasi[b]
Department of Engineering and Applied Science, Yale University, New Haven, Connecticut 06520

(Received 27 May 1980; accepted for publication 12 November 1980)

Excited-state absorption has been studied in Eu^{+2}-doped CaF_2 and in Ce^{+3}-doped $Y_3Al_5O_{12}$ at room temperature and 77 K. It is shown that the conduction band of the host crystal is responsible for absorption in both systems. In Eu^{+2}: CaF_2 the excited-state absorption is caused by a transition from the fluorescence level, the $4f^6(^7F)5d\,(^2e_g)\Gamma_8$ state, to the conduction band of CaF_2. In Ce^{+3}: YAG two processes are responsible for the absorption: (1) excitation from the lowest Ce^{+3} $5d$ energy level to the conduction band of YAG and (2) transitions from the ground state of a trap to its excited states and to the conduction band of YAG. The results provide general guidelines in the search for new uv solid-state laser materials.

PACS numbers: 42.55.Rz, 78.50.Ec, 71.70.Ch, 71.25.Tn

I. INTRODUCTION

In the search for crystals which might serve as broadly tunable blue-green or ultraviolet lasers, the importance of the role of excited-state absorption as a loss mechanism has been recognized.[1,2] This paper reports the measurements of excited-state absorption of europium (+ 2) in CaF_2 and cerium (+ 3) in $Y_3Al_5O_{12}$ (YAG). The two systems exhibit different mechanisms of loss which are discussed in detail. Generalizations of the results provide guidelines which are useful in the search for solid-state laser systems, particularly in the shorter-wavelength regions.

II. EUROPIUM (+ 2), CaF_2 SYSTEM

A. Absorption and fluorescence spectra

In single crystals of calcium fluoride doped with europium (+ 2), the impurity ion occupies a cubic site in place of a Ca^{+2} ion. The absorption spectrum, which has been known for a long time,[3] is reproduced in Fig. 1. The intense band ranging from 320 to 400 nm results from an electric dipole transition between the $4f^7$ ground state and the first excited state, which has the configuration $4f^6 5d\,(e_g)$. A second intense band beginning at ~250 nm has been attributed to the $4f^7$ to $4f^6 5d\,(t_{2g})$ transition. These assignments yield a reasonable cubic field-splitting parameter, Δ.

With uv irradiation, a strong blue fluorescence occurs with $\lambda_{max} = 420$ nm and a half-width of 22 nm. The fluorescence lifetime is 0.8 μsec, and the quantum efficiency is 0.62. If a four-level laser is assumed, lasing should occur with a threshold of 0.1 mJ if the 337-nm line of a nitrogen laser is used.[4] With considerably higher fluxes, laser action was not observed and it was presumed that excited-state absorption was likely to be an important loss mechanism.

B. Electronic energy levels

It is helpful to review the details of the electronic states of Eu^{+2} in CaF_2. The free-ion spectra have been analyzed by Sugar and Spector.[5] The ground-state term, $^8S\,(4f^7)$, is split by second-order spin-orbit coupling and the crystal field into three closely spaced energy levels, which for present purposes may be considered degenerate. Two lower spin multiplicity states of the $4f^7$ configuration, ^6P and ^6I, are found at 28 000 and 31 000 cm^{-1} above the ground state. Electric dipole transitions are forbidden between the ^8S and these states. However, Fritzler and Schaack[6] have recently reported two-photon absorption at 24 100 and 28 000 cm^{-1} in CaF_2: Eu^{+2}. The lines were assigned as the $^8S_{7/2}$ to $^6P_{5/2,7/2}$ transitions. The relationship of these states to the absorption and fluorescence is shown in Fig. 2.

Figure 2 also shows the $4f^6(^7F)5d$, $4f^6(^7F)6s$, and $4f^6(^7F)6p$ manifold of states. Electric dipole transitions from the ground state to the $5d$ manifold are parity allowed, but transitions to the $6s$ or $6p$ states are expected to be weak even with the configurational mixing.

A complete analysis of the cubic field effect on the

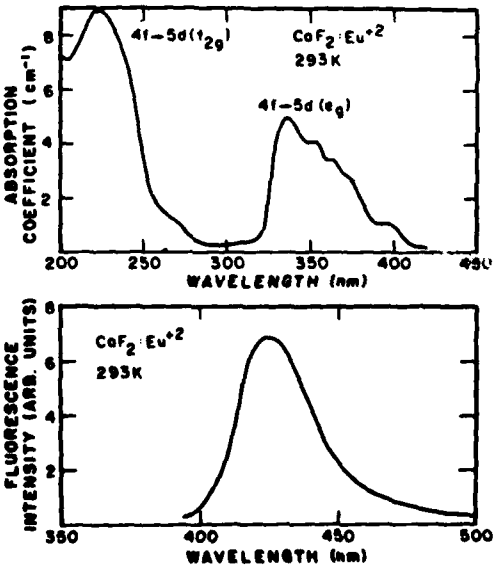

FIG. 1. The room-temperature absorption and fluorescence spectra of Eu^{+2}: CaF_2. The assignments of the transitions are those of Loh (Ref. 3).

[a] On leave from Department of Chemistry, Brandeis University, Waltham, MA 02254.
[b] Present address: Research Institute of Electrical Communication, Tohoku University, Sendai, Japan.

 0021-8979/81/1218-0880$01.10

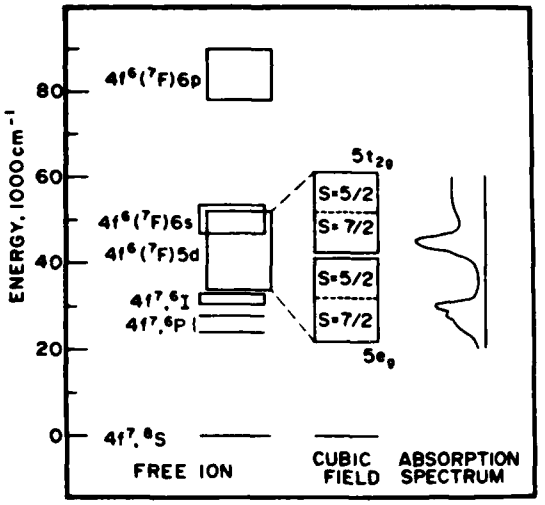

FIG. 2. A schematic diagram of the energy levels of Eu^{+2} and Eu^{+2}: CaF_2. The data for the free ion are those of Sugar and Spector (Ref. 5).

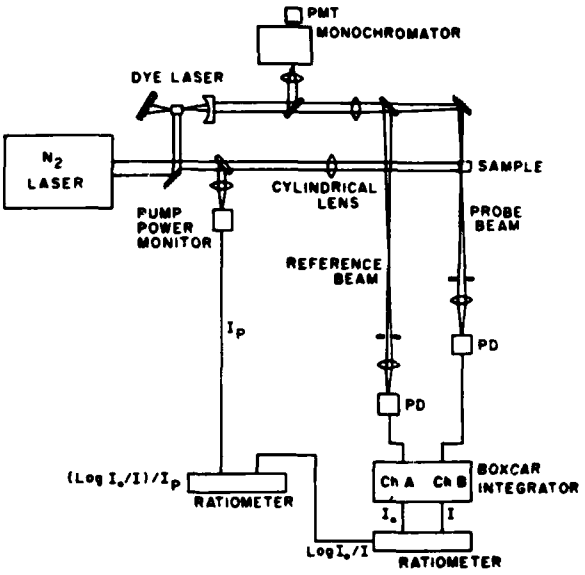

FIG. 3. A drawing of the apparatus used to measure the excited-state absorption of Eu^{+2}: CaF_2. PD is a pin diode detector. The path lengths of the reference and probe beam are the same.

manifold of $4f^6(^7F)5d$ states is yet to be done because of the extraordinary number of states. However, reasonable considerations give the following picture, diagramed in Fig. 2: The d states are split into t_{2g} and e_g states with an energy separation Δ. This has the effect of raising by $\frac{3}{5}\Delta$ and lowering by $-\frac{2}{5}\Delta$ bands whose widths are approximately that of the free-ion d band. Weakliem[7] has performed a detailed calculation for the $4f^6(^7F)e_g$ configuration as a function of an exchange parameter G_1. For a reasonable value of G_1, the plethora of states groups into two further bands which are characterized by $S = \frac{1}{2}$ and $S = \frac{3}{2}$, with an average separation of $\sim 10\,000\ cm^{-1}$. It is assumed that the selection rule, $\Delta S = 0$, is largely obeyed, and therefore the absorption band beginning at $20\,000\ cm^{-1}$ and ending at $30\,000\ cm^{-1}$ results from the $^8S_{7/2}$ to the $S = \frac{1}{2}$ states of the $4f^6(^7F)e_g$ configuration.

The blue fluorescence has been shown by Chase to be from the lowest state of the $4f^6(^7F)e_g$ manifold.[8] Using optically detected magnetic resonance, he demonstrated that this state has the symmetry $^2E(\Gamma_8)$. When this system is pumped with a nitrogen laser, $\tilde{\nu} = 29\,600\ cm^{-1}$ (337 nm), there is rapid relaxation to the $^2E(\Gamma_8)$ level from which a radiative transition to the ground manifold occurs. It will be demonstrated that strong absorption with a maximum at $19\,300\ cm^{-1}$ also occurs from the $^2E(\Gamma_8)$ state and effectively prevents laser action.

C. Experimental

The apparatus used for measurement of excited-state absorption is diagramed in Fig. 3. The beam of a Lambda-Physik nitrogen laser was split to provide a pump source for a dye laser and a pump beam to excite the Eu^{+2} into the $^2E(\Gamma_8)$ state. The short-cavity dye laser with suitable dyes gave a probe beam whose wavelengths ranged from 360 to 700 nm. The beam was focused to a 0.8-mm-diam waist at the crystal sample and was made to overlap with the 1.0-mm-diam transverse pump beam. The positions and widths of the pump and probe beams were determined by observing the shadows of the crystal as it was translated with a micrometer stage. The pump beam profile was measured with a diode array. The total pump energy irradiating the crystal was 0.32 mJ in a 3-nsec FWHM pulse.

The geometrical arrangement and the characteristics of the nitrogen and dye lasers determined the temporal relationships of the two beams at the crystal. The dye laser pulse (2-nsec FWHM) lagged the pump pulse by 3.0 nsec. Thus, the probe beam sampled the population of the excited state after over 90% of the pumping action had occurred.

The probe beam and the reference probe beam were detected with pin diodes 60 cm from the CaF_2 sample. The detection of fluorescence was minimized by using small irises in the beam paths. Signals from the probe and reference probe detectors were fed into the two channels of a PAR boxcar averager followed by a PAR ratiometer. The signals were equalized with the pump beam off. With the pump beam on, the output of the ratiometer gave $\log_{10}(I_0/I)$ directly. To eliminate variations resulting from changes in the pump intensity, a sample of the pump beam was detected and, in another ratiometer, a signal proportional to $[\log_{10}(I_0/I)]I_P$ was obtained.

D. Results and discussion

The excited-state absorption of Eu^{+2}: CaF_2 is shown in Fig. 4 for room temperature and 77 K. Since the usual absorption spectrum has no peaks below $24\,300\ cm^{-1}$ (410 nm), the observed strong transition at $19\,000\ cm^{-1}$ must originate from a state produced by the pump radiation. To show this more conclusively, measurements of $\ln(I_0/I)$ were made as a function of pump energy. The linear relationship, shown in Fig. 5, demonstrates that the concentration of excited states is linearly dependent upon the pump intensity.

Figure 6 shows the origin of the excited-state absorption. The 337-nm pump beam is absorbed into the $4f^6 5e_g$

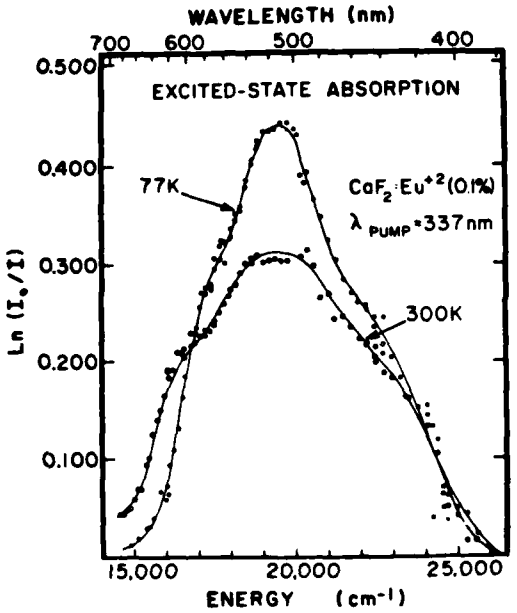

FIG. 4. The measured excited-state absorption in 0.1% Eu^{+2} : CaF_2 at room temperature and 77 K. Care was taken to assure that the measurement of $\ln(I_o/I)$ using different dyes was the same for the overlapping wavelength regions.

band of closely spaced levels, and vibrational relaxation, with a short relaxation time (several picoseconds), to the lowest $^2E_g(\Gamma_8)$ state occurs. That this process is rapid was demonstrated by observing the pump pulse scattered from the crystal and the crystal luminescence simultaneously with a single detector and fast oscilloscope. There was no measurable time delay between the maxima of the pump pulse and the luminescence. Absorption of the probe beam is caused by transitions from the ^2E_g state to another manifold of states.

If these processes are considered in conjunction with the fluorescence-absorption spectral diagram in Fig. 7, it is

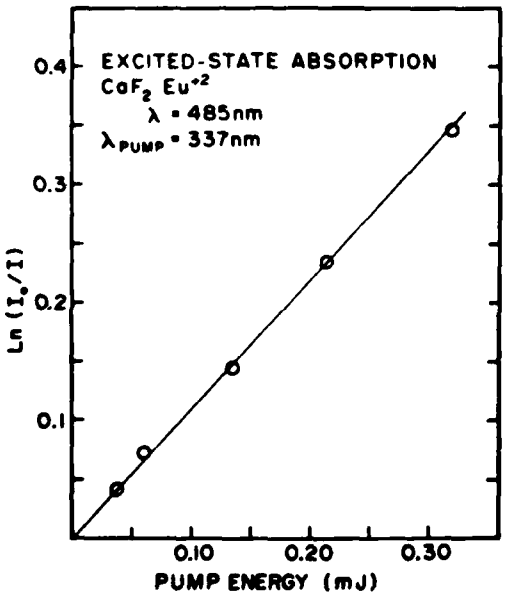

FIG. 5. A plot of $\ln(I_o/I)$ as a function of pump energy at a probe wavelength of 485 nm for Eu^{+2} in CaF_2.

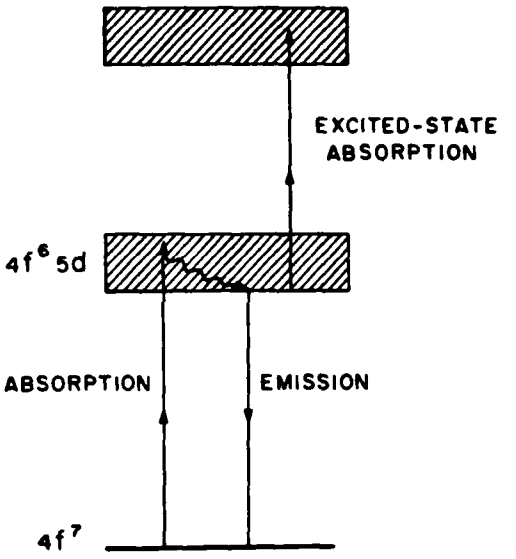

FIG. 6. A schematic drawing of the energy levels of Eu^{+2} in CaF_2 and the processes involved in excited-state absorption.

seen that the energy of the excited-state absorption, ω_1, plus the energy of the zero-phonon absorption of the $^2E(\Gamma_8)$ state, ω_2, is equal to the energy of the strong absorption band which has a peak at about 44 000 cm^{-1}. Figure 8 is a comparison of the 77 K excited-state absorption with the normal spectrophotometric absorption obtained by Loh[3] at the same temperature. The similarity of the spectral distribution is striking. It is, however, unlikely that the upper states in the excited-state absorption is the $4f^6 5t_{2g}$ manifold since this transition is expected to be quite weak from consideration of parity selection rules.

A calculation of the oscillator strength of the excited-state absorption has been performed. In the calculation, the approximation is made that the relaxation of the electrons to the lowest excited state is instantaneous and that the probe beam samples the pumped volume after the pumping is completed in a time much shorter than the relaxation time to the ground state. A sketch of the geometry of the experiment is

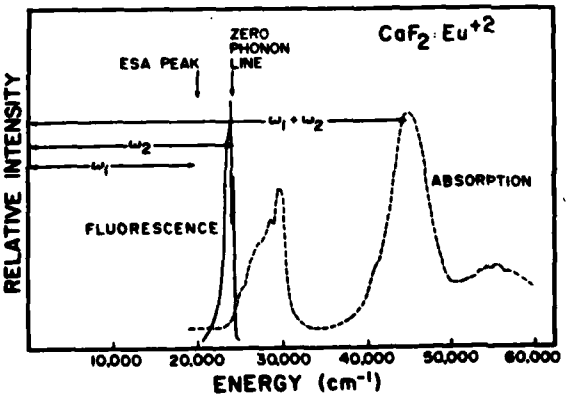

FIG. 7. A spectrum of the normal absorption and fluorescence of Eu^{+2} in CaF_2. The sum of the excited-state absorption energy, ω_1, and the zero phonon energy, ω_2, is equal to the energy of the normal absorption at 44 000 cm^{-1}.

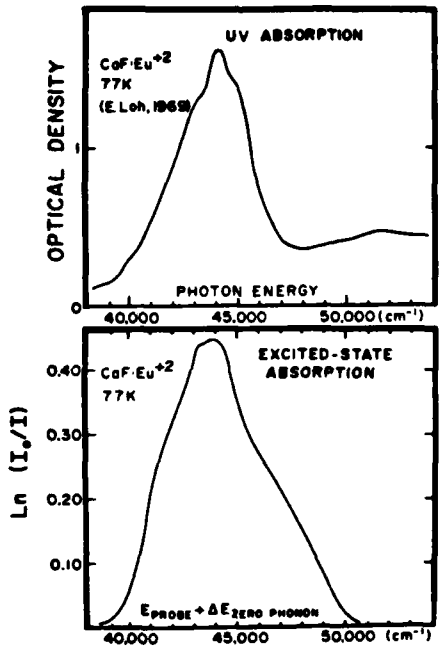

FIG. 8. A comparison of the uv normal absorption and the excited-state absorption at 40 000 cm^{-1} of Eu^{+2} in CaF_2 at 77 K.

shown in Fig. 9. The concentration of excited states produced in a volume $Lhdx$ is as follows:

$$C_x = \beta\, dP/(Lhdx), \tag{1}$$

where β is the quantum efficiency and dP is the number of pump photons absorbed in the volume unit. Since $dP/dx = -\alpha P$, where $\alpha = 8.3\ cm^{-1}$ for 337 nm,

$$C_x = (\alpha\beta/Lh)P_0 \exp(-\alpha x). \tag{2}$$

If the probe beam, intensity I_0, passes through the crystal parallel to L, then

$$\ln(I_0/I) = kC_x L, \tag{3}$$

where k is the molar extinction coefficient, and this gives

$$k = \ln(I_0/I)(h/\alpha\beta)P_0^{-1} \exp(\alpha x). \tag{4}$$

Using the values of parameters given, the maximum molar extinction coefficient is 1.65×10^4 liter $mole^{-1}$ cm^{-1}. The oscillator strength[9] is given by

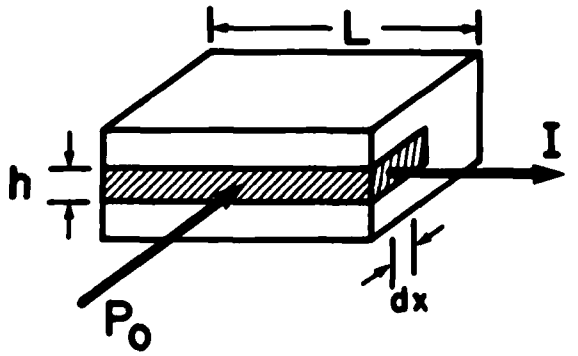

FIG. 9. A sketch of the geometry of the probe beam I and the pump beam P_0 relative to the crystal of CaF_2 containing Eu^{+2}. The volume sampled by the probe beam was always smaller than that of the pump beam.

$$f = 1.875\times10^{-9}\times[9n_0/(n_0^2+2)^2]\int k(\bar{\nu})\,d\bar{\nu}, \tag{5}$$

where n_0, the index of refraction, at 500 nm is 1.45. Graphical integration yields an oscillator strength of 0.13, which indicates that this transition is allowed. Since an e_g to t_{2g} transition is forbidden, another explanation for the absorption is required.

Recently, Pedrini, McClure, and Anderson reported on the photoionization thresholds of divalent rare-earth ions in alkaline earth fluorides.[10] They identified this energy as the difference between the lowest impurity level of the rare earth and the conduction band of the alkaline earth fluorides. For CaF_2, the band gap is 12.2 eV.[11] Although it might be expected that transitions to the CaF_2 conduction band from a rare-earth ion may be ignored, Pedrini *et al.* showed that for Tm^{+2}, Ho^{+2}, and Dy^{+2} in CaF_2, the impurity level is only about 1.7–2.7 eV below the conduction band.

Calculations using the model of Pedrini *et al.* were done for Eu^{+2}: CaF_2 using Eu^{+2}-F^- distances reported by Baberschke[12] and the known ionization potential[5] for Eu^{+2}. The calculated photoionization threshold is 4.86 eV, or about 39 000 cm^{-1}. Thus, the onset of the transitions between the impurity ion ground state and the CaF_2 conduction band coincides with the lowest energy of the excited-state absorption shown in Fig. 8. It is proposed that the strong excited-state absorption is a transition from the $^2E_g(\Gamma_8)$ state to the conduction band. Further work will be necessary to prove this assertion.

Three conclusions, which may serve as guidelines in the search for broadband tunable laser materials, can be drawn from the results of the experiment: (1) Excited-state absorption is likely to occur if the sum of the energy of the probe beam and the energy of the zero phonon fluorescence level is equal to the energy of a normal absorption band. Thus, in order to avoid excited-state absorption, twice the expected laser frequency should correspond to an energy for which there is no normal absorption. (2) Host materials should be selected with large band gaps, and the impurity ion ground-state energy should be low relative to the conduction band energy. This restricts consideration to fluorides and possibly some oxides and chlorides. (3) Many electron atoms ought to be avoided since the abundance of excited states increases the possibility of absorption compared to that of an ion with a single electron outside the core.

III. CERIUM (+3), $Y_3Al_5O_{12}$ SYSTEM

The yellow crystals of the $Y_3Al_5O_{12}$ (YAG) doped with Ce^{+3} would seem to be good laser materials. The Ce^{+3} ion, with a single electron outside its closed shell, has a simple energy level diagram, and the YAG host has a moderately large band gap of ~6 eV. However, Miniscalco *et al.*[1] and Jacobs *et al.*[2] have shown that excited-state absorption is large throughout the visible region and intensifies as the probe wavelength becomes *longer* than 600 nm, reaching a maximum beyond 700 nm.

With reference to conclusion (1) of Sec. II D, the sum of the zero phonon energy of the fluorescence band (~20 000 cm^{-1}) and the energy of the excited-state absorption peak

($\sim 14\,000\ cm^{-1}$) does not correspond to the energy of a normal absorption band. Because of this apparent contradiction, we reinvestigated this system with our apparatus.

A. Absorption and fluorescence spectra

The room temperature absorption[13] and fluorescence[14] spectra and an energy level diagram for Ce^{+3}: YAG are shown in Fig. 10. The bands are few in number and result from transitions from the ground state, $4f^1$ configuration, to the crystal field split $5d^1$ states. Recently, Robbins[15] has observed the no-phonon transitions of the lowest two bands at 489.16 and 347.21 nm. A bright yellow fluorescence results if the crystal is excited with the 337-nm radiation from a nitrogen laser. Figure 10 shows that this transition is from the lowest d level to the ground-state $4f^1$ manifold.

B. Energy levels

Ce^{+3} in YAG occupies a Y^{+3} site which has only D_2 symmetry. Therefore, all degeneracy except Kramer's degeneracy is removed. There is some similarity to the previous CaF_2 example in that each Ce^{+3} is surrounded by eight oxygens in an arrangement which is nearly cubic. Consequently, the ground-state splitting of the $^2F_{5/2,7/2}$ terms is nearly that of a cubic environment and is only a few hundred wave numbers. The states of the $5d^1$ configuration are widely split and lowered from the free-ion energy at 51 000 cm^{-1}.[16] A $6s$ state for the free ion is at 87 000 cm^{-1}. If a calculation is made for a single d electron in a cubic and axial crystal field with a spin orbit constant of 1000 cm^{-1}, then a fit to Robbins' no-phonon lines[15] predicts the remaining three no-phonon absorptions to be at 245, 243, and 213 nm. These energy levels are shown in Fig. 10.

The band gap of YAG for a number of crystals studied by Slack *et al.*[17] is about 50 000 cm^{-1} although the onset of absorption occurs at about 35 000 cm^{-1}. The optical spectra of our crystals were similar to previously published results[1,2] and showed an onset of strong absorption at 30 000–35 000 cm^{-1}, which obscures the higher-energy absorption of Ce^{+3}.

C. Results and discussion

The measurement of excited-state absorption of Ce^{+3} in YAG in the energy range 14 500–27 000 cm^{-1} was made with the same apparatus as that used for the studies of Eu: CaF_2. Room-temperature results, plotted in Fig. 11, exhibit essentially the same absorption as previously reported.[1,2] Two different crystals were used, one with 0.3 mol% Ce and the other with 0.02 mol%. The latter, a thin platelet, was used in the region of strong normal absorption. For this sample, the probe beam was redirected to form a 45° angle with the pump beam, which was focused to a 1-mm spot. Measurements of $\ln(I_0/I)$ were made in spectral regions which overlapped those of the thick crystal, and the results were scaled to form the continuous curve in Fig. 11. If a calculation of the extinction coefficient similar to that done for Eu: CaF_2 is made for Ce^{+3}: YAG at 520 nm, using a unity quantum efficiency and an absorption coefficient at 337 nm of 35 cm^{-1}, the value of k is 7.0×10^4 liter $mole^{-1}$ cm^{-1}. This again implies a large oscillator strength. It would appear that the strong nonstructural excited-state absorption is caused by the transition from the level associated with the no-phonon line at 20 400 cm^{-1} (489 nm) to the conduction band of YAG.

Experiments at low temperature tend to support this conclusion and also shed light on the origin of the long-wavelength excited-state absorption, for which there is no similar feature in the normal absorption curve. At 77 K, unusual relaxation processes show that the excited-state ab-

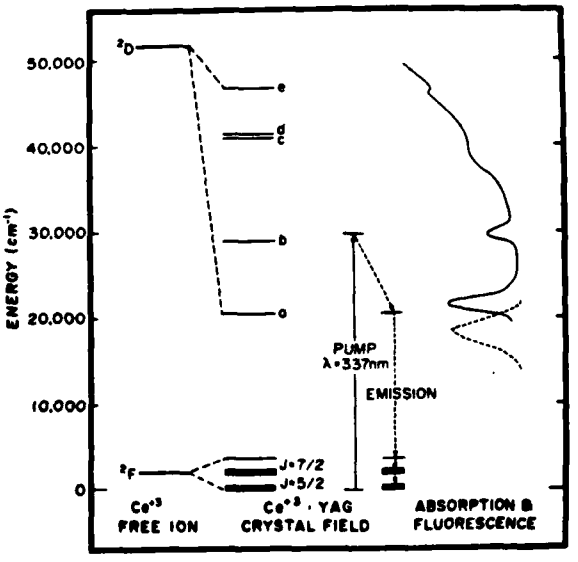

FIG. 10. The energy levels of the Ce^{+3} free ion and Ce^{+3} in YAG. Also indicated are the simple nitrogen laser pumped excitation and fluorescence processes and the normal room-temperature absorption and fluorescence spectra.

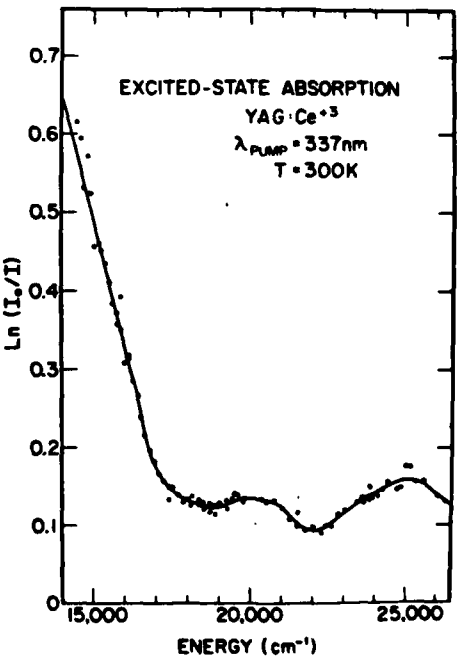

FIG. 11. The excited-state absorption spectrum of Ce^{+3} in YAG single crystals at room temperature.

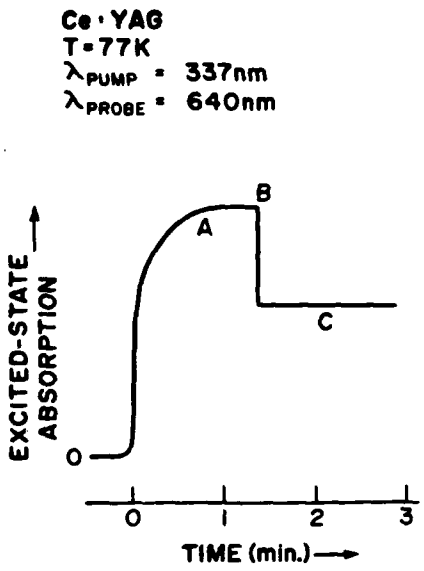

FIG. 12. The time dependence of the intensity of excited-state absorption for Ce in YAG at 77 K with $\lambda_{probe} = 640$ nm.

sorption is not a single-step process. The graph shown in Fig. 12 illustrates the multiple decay times observed with the apparatus of Fig. 3. In these measurements, the pulsed probe beam sampled the crystal a few nanoseconds after its irradiation by the 3-nsec 30-Hz pump pulses. Before $t = 0$, in Fig. 12, the pump beam is blocked and there is no absorption. The beam stop is removed at $t = 0$ and excited-state absorption rises to a plateau. At B the pump is again blocked, and the absorption drops to an intermediate value which, for a probe wavelength of 640 nm, has nearly an infinite relaxation time. In region C, the crystal phosphoresces with a spectrum characteristic of the yellow fluorescence. The decay of the phosphorescence was measured at 499 nm and at least two lifetimes, 165 sec and 11 min, were observed. Warming the crystal slowly produced thermoluminescence peaks at 97, 130, and 161 K, similar to the results obtained by Robbins *et al.*[18]

It was found that the absorption of the long-lived species could be bleached with a tungsten lamp, but no decay was observable if the probe beam wavelength was greater than 600 nm. This stability meant that the absorption could be measured by more conventional means. The crystal at 77 K was placed in the sample chamber of a Beckman spectrophotometer and spectra were run before and after nitrogen laser irradiation. These transmission curves, as well as the difference between the curves, which corresponds to the contribution to the absorption by the highly stable species, are shown in Fig. 13. Since irradiation with energies greater than 16 000 cm^{-1} causes bleaching, the trap responsible for the absorption must be about 16 000 cm^{-1} below the conduction band. The long-lived absorption is due to an allowed transition from the ground state of the trapped species to another manifold of states.

In an additional experiment, the lifetime of the "fast" component of the excited-state absorption was measured. The pulsed probe beam of Fig. 3 was replaced with the cw beam of a He-Ne laser. The boxcar amplifier was used in the

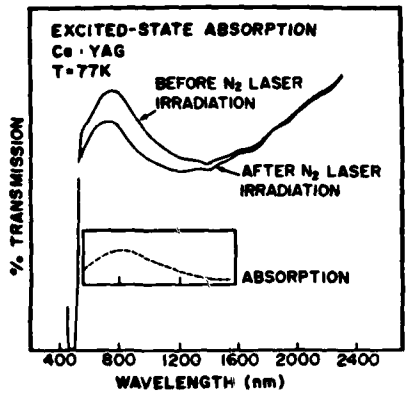

FIG. 13. The transmission curves for Ce in YAG at 77 K before and after irradiation with nitrogen laser at 337 nm. Shown in the inset is the difference in transmission, which corresponds to absorption by a stable trap.

sweep mode with a 5-nsec window, and log I was recorded. The fluorescence was observed in a similar fashion with the He-Ne laser beam blocked. The relaxation time of the excited-state absorption was characterized by a single decay time of 70 nsec, which was within a standard deviation of the measured fluorescence decay time and was independent of temperature from 77 to 298 K.

The same experimental configuration was used to measure the magnitude of the "fast" and "slow" components of the excited-state absorption at 77 K as a function of the pump energy. The results, presented in Fig. 14, show a simple linear relationship, and, therefore, simultaneous multiphonon processes are not important.

Figure 15 is an energy-level diagram which incorporates these experimental results. Pump radiation excites electrons from the $4f^1$ states to the phonon coupled states, level 3, and relaxation occurs on a picosecond time scale to the $5d$ state, level 2. Further relaxation with an estimated lifetime of 2 nsec occurs to a lower $5d$ state, level 1. As population builds in each state, pumping into the conduction band occurs. Since the fast component of the excited-state absorption has the same lifetime as the original level of the

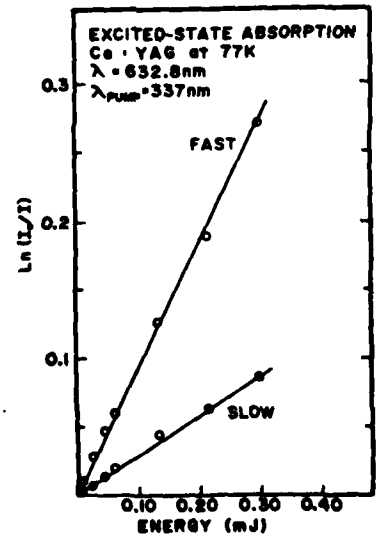

FIG. 14. The variation of $\ln(I_0/I)$ for the "fast" and "slow" components of the excited-state absorption of Ce in YAG at 77 K as a function of pump energy.

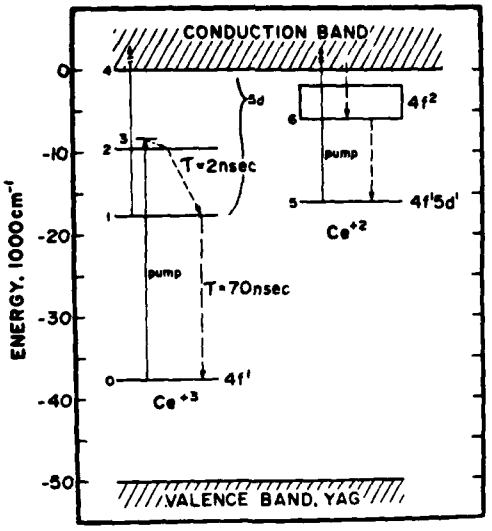

FIG. 15. An energy-level diagram for Ce^{+3} and Ce^{+2} in YAG at 77 K. The energies are given relative to the conduction band at 0 cm^{-1}. Since phosphorescence occurs, the diagram for Ce^{+3} is adjusted to make the lowest $5d$ level below the lowest Ce^{+2} level.

luminescence, it is evident that the excited-state absorption is from level 1 into the conduction band.

The origin of the slow component of the excited-state absorption cannot be explained as definitely. It is well known that numerous electron traps exist in pure crystals of YAG.[18,19] Some occur only 100–3600 cm^{-1} below the conduction band,[18] while others are much deeper. Mori[19] has studied the production of color centers in undoped YAG by uv irradiation as well as by additive coloration with aluminum and hydrogen. In each case, he observed a three-line spectrum which was assigned to an oxygen vacancy with a bound electron. This O_h^- center is similar to the alkali halide F center but, since the symmetry is low, there are three distinct absorptions corresponding to the three transitions from the s-like ground state to the three p-states. Since the lowest absorption, at 12 000 cm^{-1}, is not unlike the slow absorption shown in Fig. 13, production of O_h^- centers in Ce : YAG could explain the origin of the long-lived excited-state absorption. The other O_h^- absorptions, at 20 000 and 28 000 cm^{-1}, are weaker but presumably give rise to a slow component of excited-state absorption in the same spectral regions. Production of O_h^- centers in Ce : YAG would result from ionization of Ce^{+3} ions by each pump pulse, creating a number of electrons in the conduction band. These electrons can be trapped either by oxygen vacancies or by the Ce^{+4} ions. After numerous pumping cycles have occurred, a steady-state concentration of O_h^- centers is established.

A less conventional model, illustrated in Fig. 15, may be constructed if it is assumed that Ce^{+3} is a trap for electrons to form Ce^{+2}. It is known that Ce^{+2} in CaF_2 is stable,[20] and in YAG, with its similar environment of eight anions, it is possible that stability also occurs. From studies of the molecule CeO, an ionic radius for Ce^{+2} of 1.0 Å can be estimated.[21] This size is not much different from that of Ce^{+3} or Y^{+3}, so that the stability of Ce^{+2} in YAG depends upon a balance between the unknown Madelung energy and the ionization potential of Ce^{+2}.

The electronic energy levels of the Ce^{+2} free ion have been analyzed by Sugar.[22] The ground states, which arise from a $4f^2$ configuration, are mainly less than 7000 cm^{-1}. The states from the $4f5d$ configuration lie between 3000 and 10 000 cm^{-1}. A medium or strong crystal field will split the $4f5d$ states sufficiently to bring the lowest-energy levels below the levels of the $4f^2$ configuration. For instance, if a simple cubic field of about 20 000 cm^{-1} is assumed, the $4f5e_g$ levels will be about 10 000 cm^{-1} below the $4f^2$ manifold. Referring to Fig. 15, level 5 of the trap is assigned as the lowest $4f5d$ state, and band 6 contains the $4f^2$ energy levels.

This study of Ce^{+3} in YAG emphasizes the role of the conduction band in excited-state absorption. The results are similar to those of the Eu^{+2} in the CaF_2 system with the added complication of effective production of new ionic species or traps in the lattice which also absorb radiation. In the search for uv laser materials, the primary guideline is that the impurity ion ground state be as low as possible in the band gap of the host. This implies that the charge, ionic radius, and the ionization potential of the impurity ion and host cation are similar. In addition, the need for a large band gap limits the host compounds to fluorides and a few oxides and chlorides. The successful operation of Ce^{+3} in $LiYF_4$ as a tunable uv laser[23] is in conformity with these guidelines.

ACKNOWLEDGMENTS

We express our appreciation to Richard K. Chang for encouragement and many helpful discussions during the course of these studies. The partial support of this work by the Air Force Office of Scientific Research (Grant No. 77-3433) is also gratefully acknowledged.

[1]W. J. Miniscalco, J. M. Pellegrino, and W. M. Yen, J. Appl. Phys. 49, 6109 (1978).
[2]R. R. Jacobs, W. F. Krupke, and M. J. Weber, Appl. Phys. Lett. 33, 410 (1978).
[3]For example: E. Loh, Phys. Rev. 184, 348 (1969); D. S. McClure and Z. Kiss, J. Chem. Phys. 39, 3251 (1963); P. Kisliuk, H. H. Tippins, C. A. Moore, and S. A. Pollack, Phys. Rev. 171, 336 (1968).
[4]T. Kobayasi, S. Mroczkowski, J. F. Owen, and L. H. Brixner, J. Lumin. 21, 247 (1980).
[5]J. Sugar and N. Spector, J. Opt. Soc. Am. 64, 1484 (1974).
[6]U. Fritzler and G. Schaack, J. Phys. C 9, L23 (1976).
[7]H. A. Weakliem, Phys. Rev. B 6, 2743 (1972).
[8]L. L. Chase, Phys. Rev. 2, 2308 (1970).
[9]W. Kauzmann, *Quantum Chemistry* (Academic, New York, 1957).
[10]C. Pedrini, D. S. McClure, and C. H. Anderson, J. Chem. Phys. 70, 4959 (1979).
[11]G. W. Rubloff, Phys. Rev. B 5, 662 (1972).
[12]K. Baberschke, Phys. Lett. A 34, 41 (1971).
[13]W. W. Holloway, Jr. and M. Kestigian, J. Opt. Soc. Am. 59, 60 (1969).
[14]G. Blasse and A. Bril, J. Chem. Phys. 47, 5139 (1967).
[15]D. J. Robbins, J. Electrochem. Soc. 126, 1550 (1979).
[16]R. Long, Can. J. Chem. A. 13, 1 (1935); 14, 127 (1936).

[17]G. A. Slack, D. W. Oliver, R. M. Chenko, and S. Roberts, Phys. Rev. 117, 1308 (1969).
[18]D. J. Robbins, B. Cockayne, J. L. Glasper, and B. Lent, J. Electrochem. Soc. 126, 1213 (1979); 126, 1221 (1979); 126, 1556 (1979).
[19]K. Mori, Phys. Status Solidi A 42, 375 (1977).
[20]R. C. Alig, Z. J. Kiss, J. P. Brown, and D. S. McClure, Phys. Rev. 186, 276 (1969).
[21]R. J. Ackermann, E. G. Rauh, and R. J. Thorn, J. Chem. Phys. 65 1027 (1976).
[22]J. Sugar, J. Opt. Soc. Am. 55, 33 (1965).
[23]D. J. Ehrlich, P. F. Moulton, and R. M. Osgood, Opt. Lett. 4, 184 (1979).

APPENDIX C

Rayleigh Scattering Measurements of the Gas Concentration Field in Turbulent Jets

M. Carla Escoda and Marshall B. Long

Yale University
New Haven, Connecticut 06520

Abstract

A technique based on Rayleigh scattering has been developed to measure the concentration field in a cross section of a turbulent gas jet. Such measurements enable one to quantitatively study turbulent mixing mechanisms and structures. A similar experiment was previously performed using Lorenz/Mie scattered light from aerosol particles introduced into the nozzle gas. The Rayleigh technique provides better spatial resolution, avoiding the limitations due to aerosol seeding, and in particular is capable of monitoring molecular diffusion, a fact which should be of importance in studying reactive turbulence.

INTRODUCTION

The need for high-resolution nonintrusive methods of obtaining quantitative information on mixing in turbulent flows has led to the development of light scattering techniques to determine molecular concentration and temperature profiles. Rayleigh and Raman scattering have proven to be particularly valuable for making measurements at single points or along a line in the flow.[1-6] However, recent interest in large-scale coherent structures in turbulence demonstrates the need for instantaneous two-dimensional measurements. The study of turbulent eddies and their relation to the large vortical structures developed further upstream in the transition region of a jet requires fine temporal and spatial resolution and the simultaneous probing of an entire flow region. In addition, turbulent mixing often takes place in environments that are relatively inaccessible or destructive to conventional probes. Since light scattering methods can monitor events in an essentially "instantaneous" manner and do not require the introduction of physical probes into the flow, they are extremely valuable to the experimental study of turbulence.

A PREVIOUS LIGHT SCATTERING TECHNIQUE

Our application of Rayleigh scattering to the two-dimensional mapping of concentration in the near field of a freon jet is similar to a technique previously developed to infer the concentration by measuring the Lorenz/Mie scattering from an aerosol-seeded jet.[7]

Both experiments utilized the fact that the intensity of scattered light is proportional to the number of scatterers in the illuminated volume, i.e., to the number of seeded particles per resolution element in the Lorenz/Mie case or to the number of gas molecules per resolution element in the Rayleigh case. The variation of scattered light intensity across a sheet of laser light in a plane of the jet is recorded with a computer-controlled low-light-level TV camera (PAR OMA-2). The scattered light intensity is interpreted as being proportional to the nozzle fluid concentration. The image is digitized at 10,000 points and stored in the computer, thus providing a measure of relative concentrations in two dimensions. Figure 1 shows a typical instantaneous concentration map (using the Lorenz/Mie technique) produced by gating the TV camera on for a time short compared to the estimated time during which detectable downstream translation occurs (10 μs).

Data acquired in this manner must be corrected to account for the background signal, the camera response, and the nonuniformity of the laser sheet. In the first part of this two-step process, a 100 x 100 "background" frame, taken without the jet on, is subtracted from the data frame. Then a rectangular glass cell holding a dilute fluorescent dye solution is placed in the path of the laser sheet so that a fluorescent sheet is imaged onto the camera face. (Optical filters are used to pass only the fluorescence.) Since the fluorescence signal is constant across the sheet, the actual recorded signal intensities reflect both the nonuniform response of the camera and the intensity distribution in the sheet, which drops off at either end in the direction of the jet axis and peaks in the center

due to the Gaussian profile of the incident beam. The background-corrected frame is finally divided by this response frame.

Although the Lorenz/Mie technique affords a high resolution (200 x 200 x 200 μm per unit resolution volume[7]), it still does not resolve finer structures known to exist in the turbulent regimes studied. Spatial resolution using the Lorenz/Mie technique is limited by marker shot noise which is inversely proportional to the root of the number of seeded aerosols per unit volume. Marker shot noise is evident in Fig. 1 from the variations in intensity between adjacent points in areas where there is no significant concentration gradient. (At this low Reynolds number of 4160, the potential core extends at least partially into the region under observation. Thus, the intensity variations toward the center of the jet in the upstream region of the profile are the result of marker shot noise and cannot represent the actual concentration profile.) In order to minimize marker shot noise, marker density must be high. Overly heavy seeding of the nozzle gas, however, may lead to multiple light scattering, i.e., the rescattering of signal from one aerosol by another before the original signal reaches the camera face. Furthermore, most of the scattering comes from the largest particles so that, in a polydisperse flow, large intensity variations between two scattering volumes under identical flow conditions may arise from a small variation in the number of large aerosols. While in a unit resolution volume measuring 200 x 200 x 200 μm there are approximately 1,000 aerosols, an increase in magnification, resulting in a smaller resolution volume, means a decrease in marker density and thus an increase in marker shot noise. In general, therefore, seeding levels restrict resolution in the Lorenz/Mie scattering technique.

The large size of aerosols relative to gas molecules limits their

ability to follow flows in which there are large accelerations. Also the instantaneous concentration distributions obtained by the Lorenz/Mie scattering technique could be misleading in regions where molecular diffusion effects are important, since the seeding particles do not diffuse. The Rayleigh experiment was expected to overcome the major noise and resolution limitations of the Lorenz/Mie technique, since scattering from molecules of the nozzle gas was measured rather than that from particles introduced into the flow.

THE RAYLEIGH SCATTERING TECHNIQUE

Because the intensity of the scattered Rayleigh signal from gas molecules is several orders of magnitude lower than that of the Lorenz/Mie signal from aerosols, the Rayleigh experiment requires higher incident laser power, a "clean" environment to eliminate scattering from particulates, and stray light suppression. In addition, it is desirable to maximize the scattering cross-section ratio between ambient and nozzle gases. This cross section depends on the incident wavelength and the refractive index as follows:[8]

$$\sigma_{R_i} = \frac{4\pi^2}{\lambda_o^4}\left[\frac{(n_i - 1)}{N_o}\right]^2 .$$

λ_o is the incident wavelength, n_i the refractive index and N_o the number density. Thus we chose a gas of high refractive index (such as freon) discharging into a gas of much lower index (e.g., air, He) to maximize the contrast between scattered signal intensities from the nozzle and ambient gases. This coflowing configuration consists of a nozzle with a diameter, d, of 6 mm surrounded by a coaxial honeycomb. To eliminate

Lorenz/Mie scattering from dust particles, we cleaned both flows using in-line microfiber filters (pore size = 0.3 μm). The experimental setup (see Fig. 2) was similar to that of the Lorenz/Mie experiment.[7] While an argon ion laser (λ_o = 488 nm) provided enough energy (20 μJ in 10 μs) for the Lorenz/Mie experiment, it was necessary to use a pulsed Nd:YAG laser (λ_o = 532 nm) that provided 20 mJ in a 15 ns pulse. The laser beam was focused into a sheet approximately 50 μm thick over the jet, and two camera lenses (57 and 135 mm focal lengths) collected and focused the scattered light from a portion of the illuminated sheet onto the face of the camera. The digitized data for each instantaneous shot were stored in an 80 x 100 array on magnetic tape.

Figure 3(a) shows a typical shot for freon discharging into nitrogen. Note the absence of marker shot noise, as compared to the Lorenz/Mie profile in Fig. 1. The coflowing jets can be characterized by the parameters $m = v_1/v_2$ (velocity ratio) and $n = \rho_1/\rho_2$ (density ratio) where 1 signifies the ambient gas and 2 the nozzle gas.[9] In this case, m = 0.18 and n = 0.20. A unit resolution volume measures 130 x 150 x 50 μm since the entire area under observation was 1.7d x 2.5d. Subsequent magnification was accomplished through switching the positions of the camera lenses and a smaller area of the jet was monitored [see Fig. 3(b)]. The spatial resolution is now 40 x 48 x 50 μm, and structures on the order of 100-200 μm are now clearly resolvable.

In the Rayleigh experiments, data were corrected for camera response and intensity distribution in the sheet by forcing the coflowing gas (in this case, N_2) through both the nozzle and the honeycomb to provide a

"constant" intensity field over the entire camera face. The "response" frame was obtained by averaging over several such frames. This correction was less successful than the one made for the Lorenz/Mie data so an additional step was taken. One column, or track, of data was chosen in the center of the data frame, as close as possible to the jet centerline (where presumably the actual intensities were fairly constant in the direction of the jet axis), and divided into each of the remaining tracks. Thus the artificial peak toward the center of each frame due to nonuniform intensity distribution in the sheet was suppressed.

Because of the refractive index difference between nozzle and ambient gases, it is conceivable that small structures in the flow would be optically distorted. Since the characteristics of the interface between the two gases are not known, the optical paths of signals from two adjacent points in the flow may be different, and defocusing would result. This would effectively limit the spatial resolution. To examine the actual effect of this index mismatch, a 10 μm optical fiber was placed perpendicular to the jet axis at the same distance downstream from the nozzle exit as in the Rayleigh experiments. The fiber was illuminated perpendicular to its axis with a lamp and the light scattered off it was focused onto the TV camera. Initially, the image of the fiber was recorded without turning the jet on. With the jet on, and under the same flow conditions as in the experiment, there was no measurable optical distortion of the fiber image. We can therefore conclude that the potential resolution-limiting mechanism arising from the density difference between the ambient and nozzle gases does not affect our experiment down to the

limit of our current resolution.

MOLECULAR DIFFUSION ANALYSIS

That the Rayleigh scattering technique presents a significant improvement over Lorenz/Mie scattering can be demonstrated by its ability to detect molecular diffusion effects. While these effects are insignificant compared to the convection of large-scale structures in non-reactive flows, they become important in reactive flows in which instantaneous (and not mean) concentration profiles determine the local reaction rate. In regimes where molecular diffusion has affected the flow, we do not expect optical diagnostic techniques based on scattering from seeded particles to reveal diffusion-related structure changes. For example, assuming infinite resolution, i.e., no marker shot noise, we expect to see sharp, clearly defined boundaries indicative of the extent to which the aerosol particles have followed the "rolling up" of vortices in the process of entrainment of the ambient gas by the nozzle fluid. In reality, we do not expect these boundaries to be so clearly defined since diffusion of the nozzle fluid must have occurred to smooth out the profile somewhat. Information on this diffusion will be available from the Rayleigh data, provided the diffusion length (i.e., the distance over which the freon has diffused) is greater than the distance between two adjacent resolution volumes.

The distance over which one gas diffuses into another depends on the time interval allowed for diffusion. According to Becker and Massaro,[10]

vortices roll up ½ revolution per wavelength of translation. In this case, the wavelength is on the order of the nozzle diameter [see Fig. 3(a)] and the vortices are convected with a speed approximately equal to the average exit speed of the nozzle and ambient gases or 3 m/s. Therefore, the time required to form a fold in a vortex is (6 mm)/(3 m/s) or 2 ms.

Treating the freon-air mixture as a binary mixture and regarding the molecules as rigid spheres, one can estimate the diffusivity D of freon in air to be roughly 0.1 cm^2/sec. In a time interval of 2 ms, the freon would therefore have diffused a distance equal to $\sqrt{2D(\Delta t)}$ or $(2 \times 0.1 \times 2 \times 10^{-3})^{\frac{1}{2}} = 200$ μm. Since the spatial resolution in the Rayleigh experiment is on the order of 50 μm, the effects of molecular diffusion should be detectable.

Experimental confirmation is provided by a direct comparison of Lorenz/Mie and Rayleigh scattering under the same flow conditions (low flow rate). Since the flow from the original nozzle could not be seeded, a 4 mm diameter nozzle was used, with freon discharging into air (m = 0). In the Lorenz/Mie experiments, freon seeded with submicron sized particles was used and, for the Rayleigh case, filtered freon was discharged into the ambient air.

A visual comparison of many instantaneous nozzle gas concentration distributions such as those shown in Figs. 1, 3(a), and 3(b) reveals clearly that, on the average, concentration distributions obtained by the Lorenz/Mie scattering technique have steeper gradients near the jet boundaries than those obtained by the Rayleigh scattering technique. The difference in steepness of the concentration profiles is clearly

demonstrated in Fig. 4. The two adjacent curves in each case represent two constant concentration contours, which are 40 and 60% of the maximum nozzle gas concentration. The average distance between the two curves is an indication of the steepness of the concentration gradient in that region. This distance is consistently larger in the case of Rayleigh scattering (under the same flow conditions) and is therefore evidence of molecular diffusion.

CONCLUSION

A technique based on Rayleigh scattering has been developed to measure the instantaneous two-dimensional concentration field in a section of a turbulent gas jet. A similar experiment was previously performed using Lorenz/Mie scattered light from aerosol particles introduced into the nozzle gas. The Rayleigh technique provides finer spatial resolution (on the order of 50 μm), avoiding the limitations due to aerosol seeding density, and in particular is capable of monitoring molecular diffusion.

Because the concentration profile can be directly inferred from the scattered intensity profile of the gas molecules themselves, it should be possible to make measurements in the far field of a jet (more than 12 diameters downstream) and to attain even finer resolution, given sufficient incident laser power. (The required laser power is inversely proportional to the number density of scattering molecules which decreases linearly with distance downstream. Thus, a shift to the far field requires an increase in incident power directly proportional to the distance of the region under observation from the nozzle exit.) With these capabilities, it should become possible to detect small scale turbulence.

ACKNOWLEDGMENTS

We thank R. K. Chang and B. T. Chu for many helpful discussions and Sandia National Laboratories (Livermore) for the loan of the burner used in this work. The partial support of the Air Force Office of Scientific Research (Grant No. 77-3433) is also gratefully acknowledged.

REFERENCES

[1]Dyer, T.M., "Rayleigh Scattering Measurements of Time-Resolved Concentration in a Turbulent Propane Jet," AIAA Journal, Vol. 17, August 1979, pp. 912-914.

[2]Pitz, R.W., Cattolica, R., Robben, F., and Talbot, L., "Temperature and Density in a Hydrogen-Air Flame from Rayleigh Scattering," Combustion and Flame, Vol. 27, 1976, pp. 313-320.

[3]Graham, S.C., Grant, A.J., and Jones, J.M., "Transient Molecular Concentration Measurements in Turbulent Flows Using Rayleigh Light Scattering," AIAA Journal, Vol. 12, August 1974, pp. 1140-1142.

[4]Smith, J.R., "Rayleigh Temperature Profiles in a Hydrogen Diffusion Flame," Proceedings of the Society of Photo-Optical Instrumentation Engineers, Vol. 158, 1978, pp. 84-90.

[5]Birch, A.D., Brown, D.R., Dodson, M.G., and Thomas, J.R., "The Turbulent Concentration Field of a Methane Jet," Journal of Fluid Mechanics, Vol. 88, 1978, pp. 431-449.

[6]Goulard, R. (ed)., Combustion Measurements, Academic Press, New York, 1976.

[7]Long, M.B., Chu, B.T., and Chang, R.K., "Instantaneous Two-Dimensional Gas Concentration Measurements by Light Scattering," AIAA Journal, Vol. 19, September 1981, pp. 1151-1157.

[8]Penney, C.M., "Light Scattering in Terms of Oscillator Strengths and Refractive Indices," Journal of the Optical Society of America, Vol. 59, 1969, pp. 34-42.

[9]Abramovich, G.N., Yakovlevsky, O.V., Smirnova, J.P., Secundov, A.M., and Krasheninnikov, S.Yu., "An Investigation of the Turbulent Jets of Different Gases in a General Stream," Astronautica Acta, Vol. 14, 1969, pp. 229-240.

[10]Becker, H.A. and Massaro, T.A., "Vortex Evolution in a Round Jet," Journal of Fluid Mechanics, Vol. 31, 1968, pp. 435-448.

FIGURE CAPTIONS

Fig. 1. Instantaneous concentration profile of a turbulent jet (seeded air exiting into air) obtained by the Lorenz/Mie scattering technique. The nozzle diameter, d, was 4 mm and the Reynolds number was 4160.

Fig. 2. Experimental configuration for the Rayleigh scattering technique. The inner nozzle has a diameter of 6 mm. Both gas streams are filtered with 0.3 μm filters to remove dust particles from the flow.

Fig. 3. Instantaneous concentration profiles of a coflowing turbulent jet (freon into nitrogen) obtained by Rayleigh scattering. In (a), the entire jet (from 4d to 8d) is imaged onto the computer-controlled TV camera. In (b), a smaller region of the jet is imaged onto the camera giving a spatial resolution of 48 x 50 x 50 μm. In both cases, the freon exit velocity was 4.6 m/s and the velocity ratio, m, was 0.18. The density ratio, n, of freon and air is 0.20.

Fig. 4. Comparison of constant concentration contours obtained from (a) Lorenz/Mie scattering and (b) Rayleigh scattering. The outer curve in each figure represents the portion of the jet where the concentration is 60% of the maximum jet concentration; the inner curve is the 40% contour. The average distance between the contours indicates the steepness of the concentration gradient. The data were for freon exiting into ambient air.

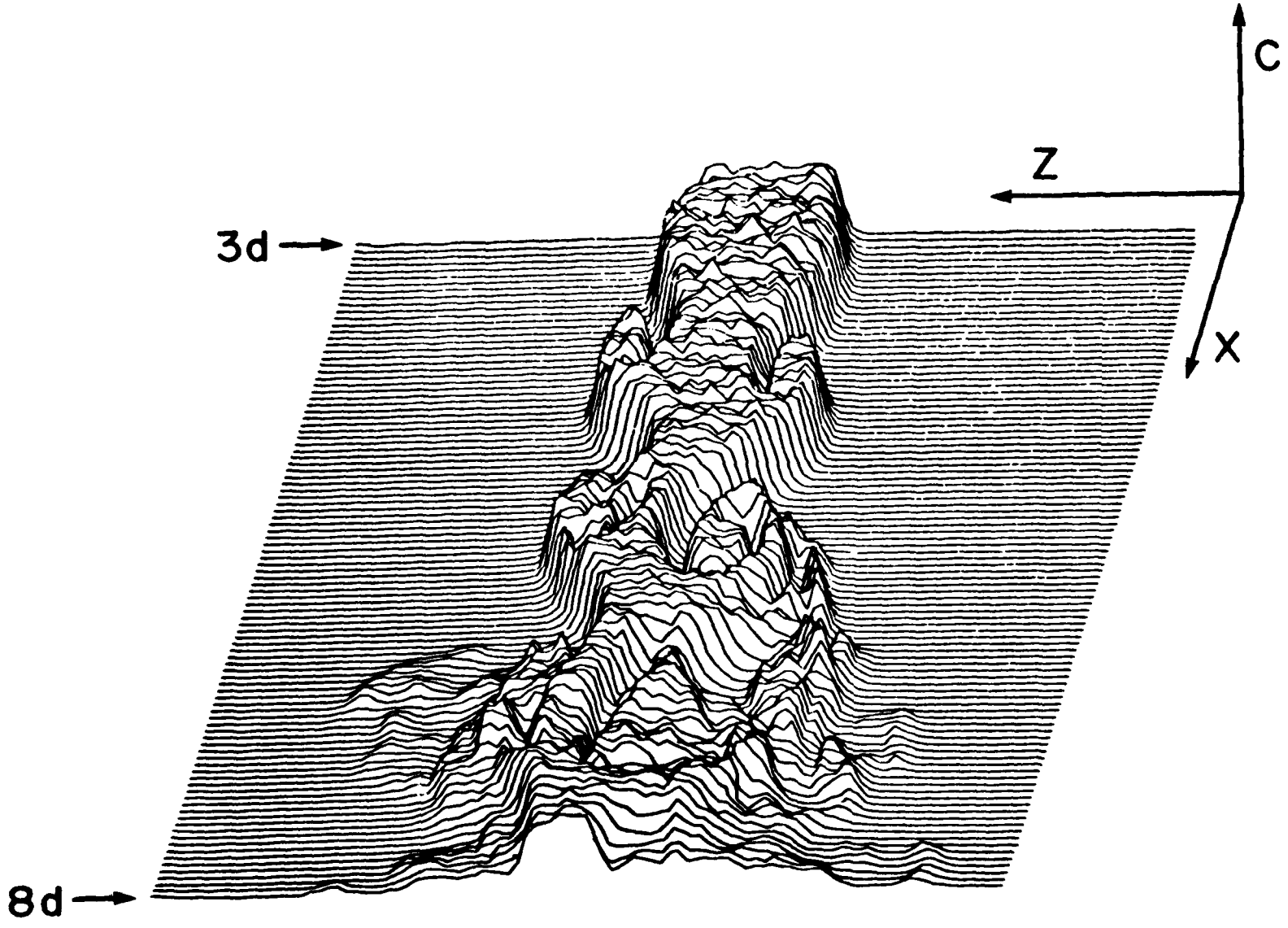

FIGURE 1

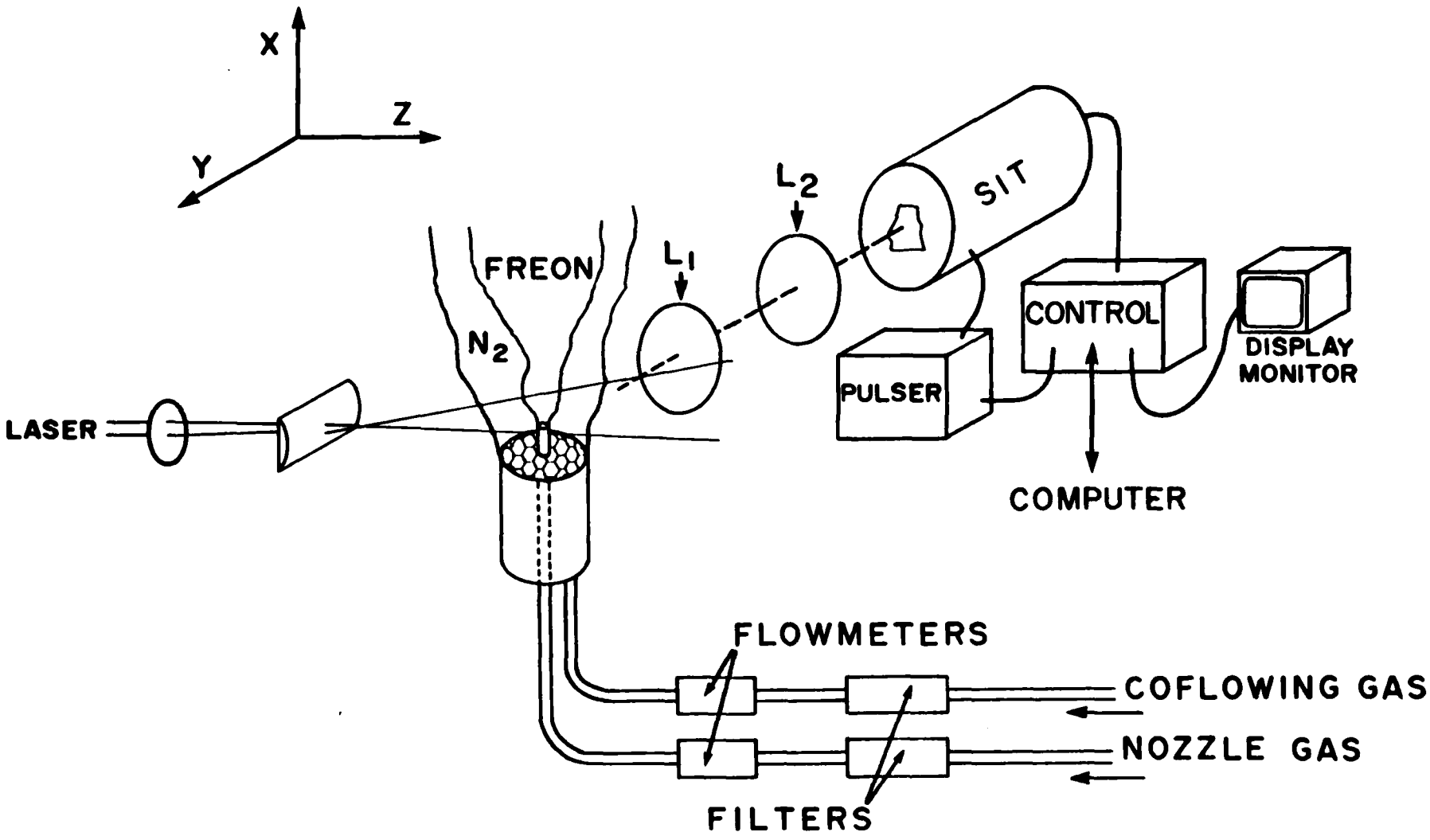
X
Z
Y
L_2
SIT
FREON
L_1
N_2
CONTROL
DISPLAY
MONITOR
PULSER
LASER
COMPUTER
FLOWMETERS
COFLOWING GAS
NOZZLE GAS
FILTERS

FIGURE 2

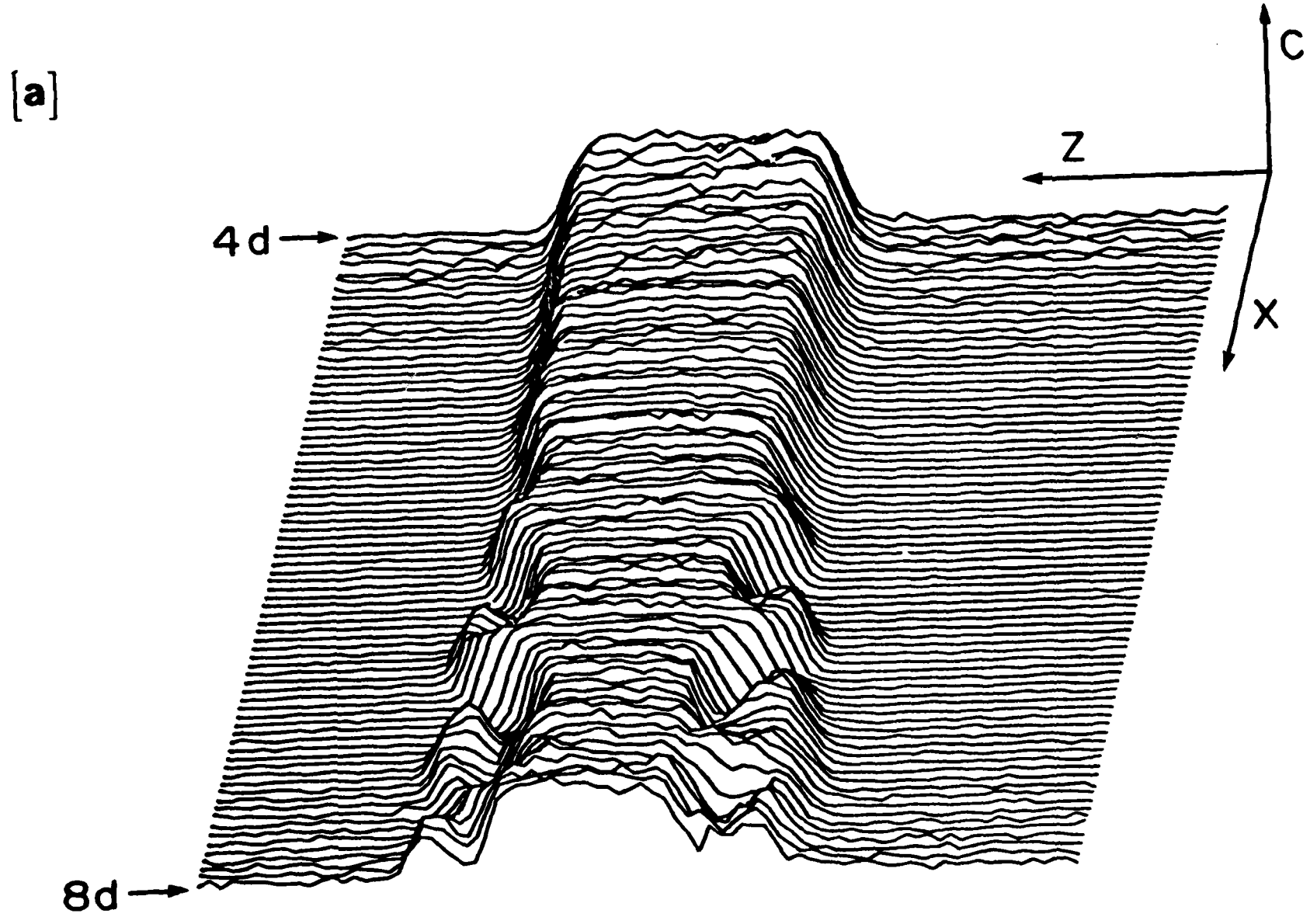

FIGURE 3(a)

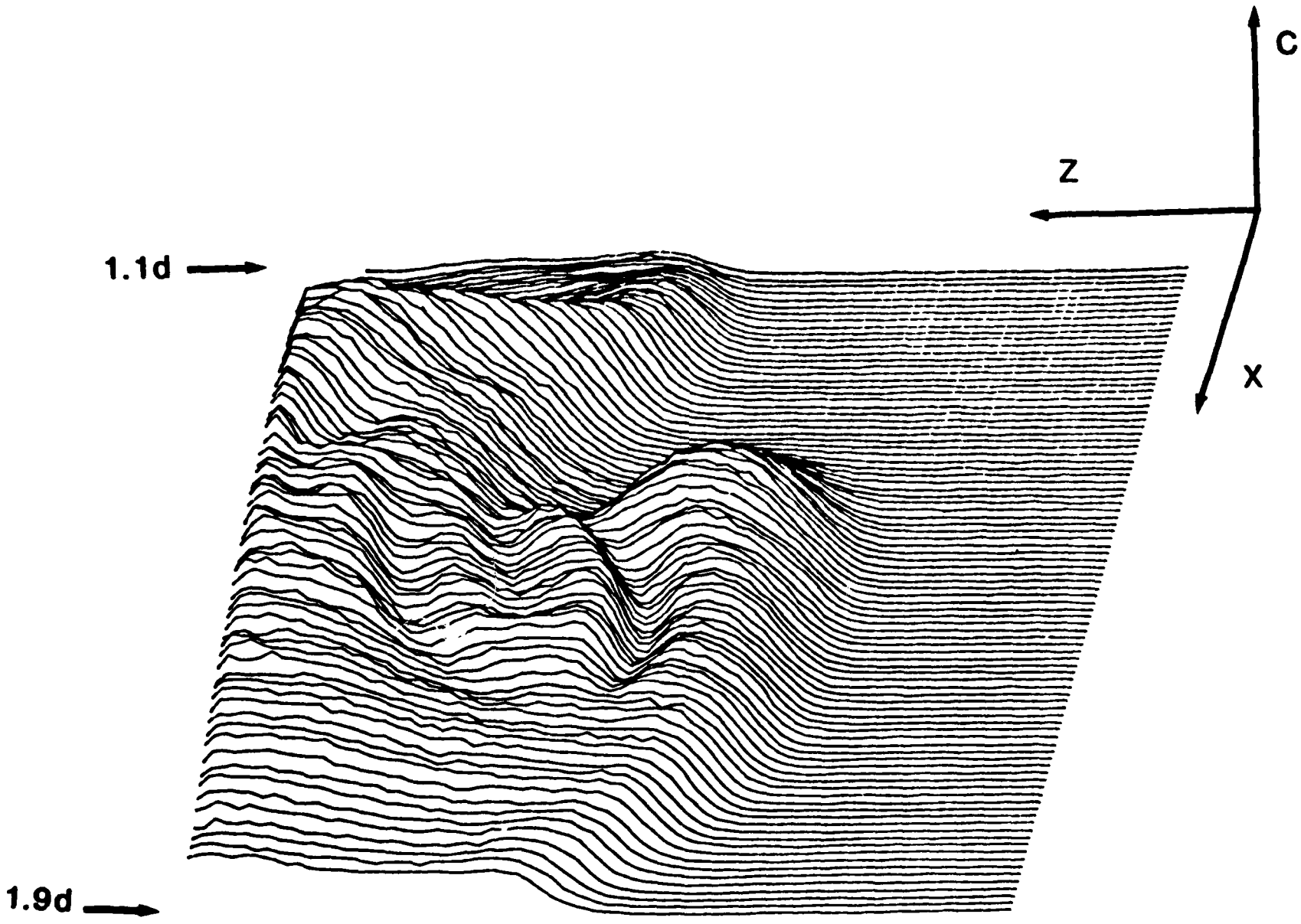

FIGURE 3(b)

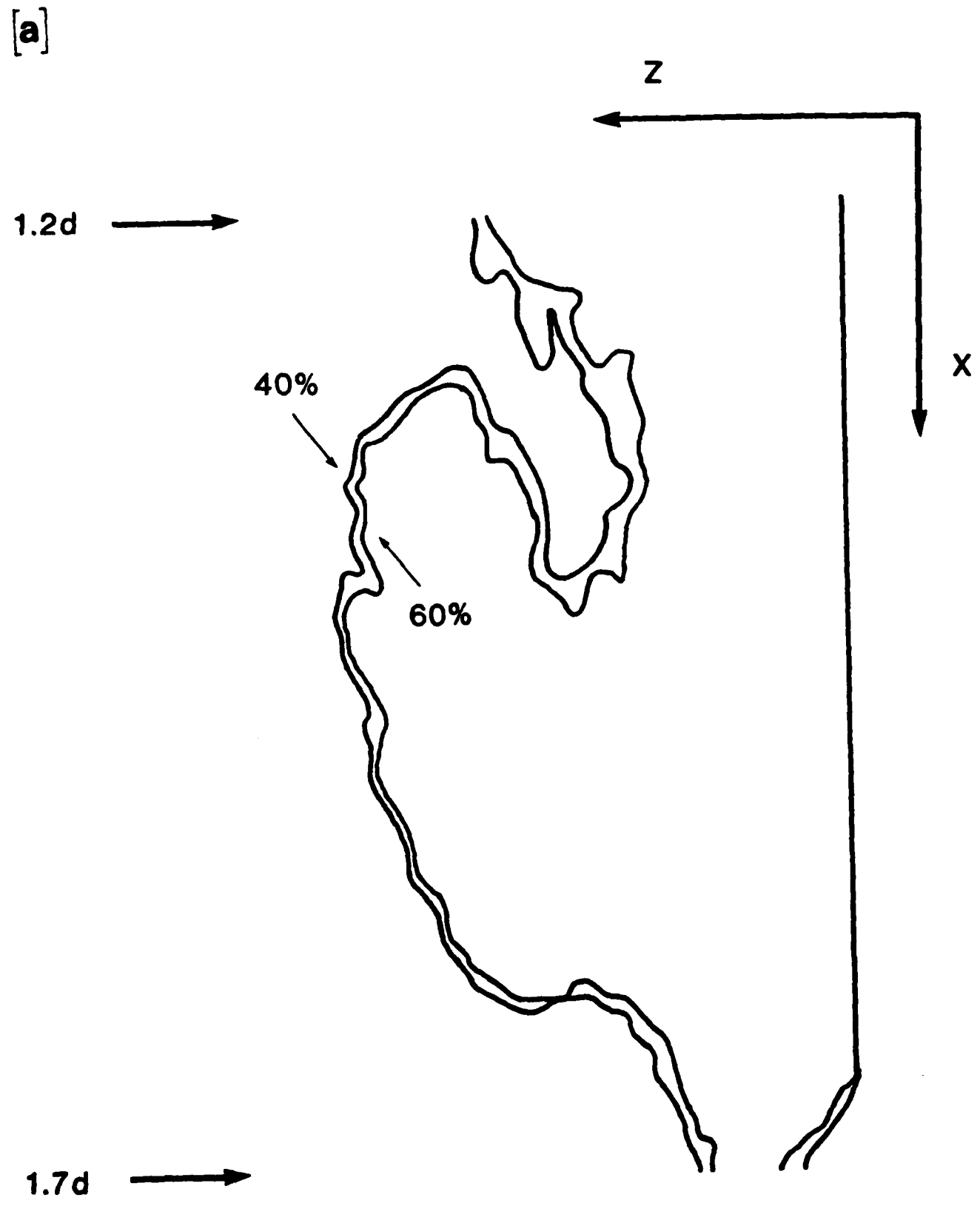

FIGURE 4(a)

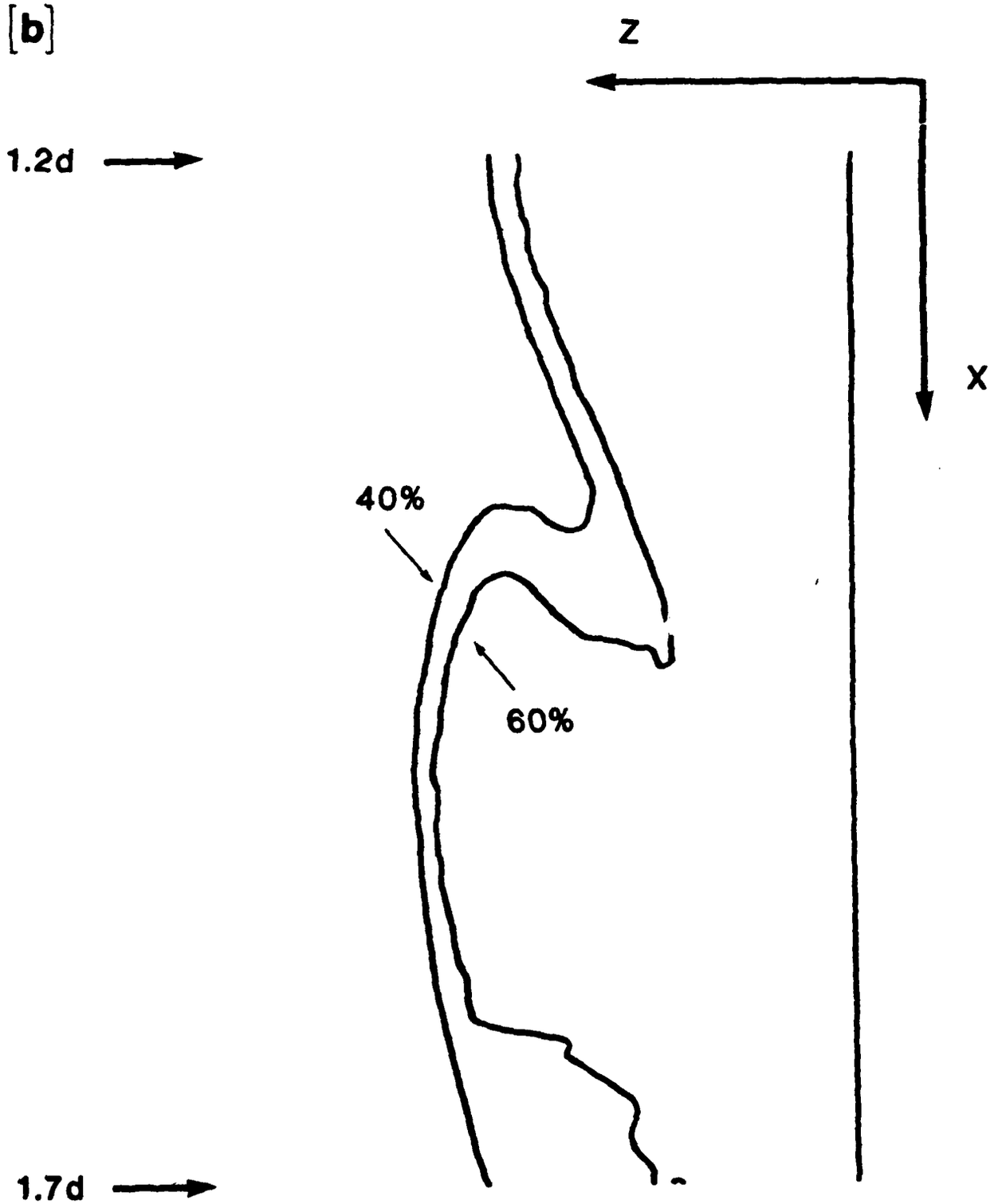

FIGURE 4(b)


DATE
ILME